



HAL
open science

The Loongana (CL) group of carbonaceous chondrites

Knut Metzler, Dominik Hezel, Jens Barosch, Elias Wölfer, Jonas Schneider, Jan Hellmann, Jasper Berndt, Andreas Stracke, J. Gattacceca, Richard Greenwood, et al.

► **To cite this version:**

Knut Metzler, Dominik Hezel, Jens Barosch, Elias Wölfer, Jonas Schneider, et al.. The Loongana (CL) group of carbonaceous chondrites. *Geochimica et Cosmochimica Acta*, 2021, 304, pp.1-31. 10.1016/j.gca.2021.04.007 . hal-03201634

HAL Id: hal-03201634

<https://hal.science/hal-03201634>

Submitted on 22 Oct 2021

HAL is a multi-disciplinary open access archive for the deposit and dissemination of scientific research documents, whether they are published or not. The documents may come from teaching and research institutions in France or abroad, or from public or private research centers.

L'archive ouverte pluridisciplinaire **HAL**, est destinée au dépôt et à la diffusion de documents scientifiques de niveau recherche, publiés ou non, émanant des établissements d'enseignement et de recherche français ou étrangers, des laboratoires publics ou privés.

The Loongana (CL) group of carbonaceous chondrites

Knut Metzler ^{a,*}, Dominik C. Hezel ^b, Jens Barosch ^b, Elias Wölfer ^a, Jonas Schneider ^a,
 Jasper Berndt ^c, Andreas Stracke ^c, Jérôme Gattacceca ^d, Richard C. Greenwood ^e, Ian A. Franchi ^e,
 Christoph Burkhardt ^a, Thorsten Kleine ^a

^a *Institut für Planetologie, University of Münster, Wilhelm-Klemm-Straße 10, 48149 Münster, Germany*

^b *Institut für Geologie und Mineralogie, University of Cologne, Zùlpicher Straße 49a, 50674 Köln, Germany*

^c *Institut für Mineralogie, University of Münster, Corrensstraße 24, 48149 Münster, Germany*

^d *CNRS, Aix Marseille University, IRD, INRAE, CEREGE, Aix-en-Provence, France*

^e *Planetary and Space Sciences Research Institute, Open University, Milton Keynes MK7 6AA, UK*

* Corresponding author at: Institut für Planetologie, University of Münster, Wilhelm-Klemm-Str. 10, 48149 Münster, Germany
 E-mail address: knut.metzler@uni-muenster.de (K. Metzler).

Abstract

A coordinated study of the petrology, mineral chemistry, and bulk chemical and isotopic composition of the five ungrouped carbonaceous chondrites Coolidge, Loongana 001, Los Vientos (LoV) 051, Northwest Africa (NWA) 033, and NWA 13400 reveals that these meteorites have a similar set of properties that distinguishes them from the other carbonaceous chondrite groups and allows definition of the new Loongana (CL) group of carbonaceous chondrites. The characteristics of the investigated samples include: (1) Fe-Ni metal abundances considerably higher than for CV chondrites, but similar to CR chondrites; (2) Chondrule size-frequency distributions similar to CV chondrites, but dissimilar to CR chondrites; (3) Mean CAI abundances of ~1.4 vol%, i.e., lower than in CV but much higher than in CR chondrites; (4) Very low amounts of inter-chondrule matrix (17-21 vol%), the lowest among the main carbonaceous chondrite groups (CI, CY, CM, CO, CV, CR, CK); (5) Nearly equilibrated olivine with mean fayalite (Fa) values of olivine between 12.5 mol% (Loongana 001) and 14.7 mol% (NWA 13400) as a metamorphic effect; (6) Lower Al₂O₃ and higher MgO and Cr₂O₃ concentrations in inter-chondrule matrix compared to matrix in CV, CK, and CR chondrites; (7) Considerable bulk depletion of volatile lithophile elements (Mn, Na, K, Rb, Cs) and chalkophile elements (Zn, Se, Te, Pb, Tl) compared to all other main carbonaceous chondrite groups; (8) Bulk O isotope compositions plotting along the CCAM line ($\Delta^{17}\text{O}$ -3.96 to -5.47‰), partly overlapping with the CV and CK chondrite field but including samples that are more ¹⁶O-rich; (9) Unique positions in the $\epsilon^{54}\text{Cr}$ - $\epsilon^{50}\text{Ti}$ isotope plot, with $\epsilon^{54}\text{Cr}$ values similar to CV and $\epsilon^{50}\text{Ti}$ values similar to CR chondrites. Taking all observations together, it can be concluded that CL chondrites are unrelated to CR chondrites but may be genetically related to CV and CK chondrites. All CL chondrites studied here are of petrologic type 3.9 to 4, indicating that they have been thermally overprinted on the parent body. The diagnostic features of CL chondrites detailed here should provide a basis for identifying CL members of lower petrologic types. Such samples would be important in determining the pristine state of these meteorites and their components.

1. INTRODUCTION

44
45
46
47
48
49
50
51
52
53
54
55
56
57
58
59
60
61
62
63
64
65
66
67
68
69
70
71
72
73
74
75
76
77
78
79
80
81
82
83

Chondrites are cosmic sediments, which consist of up to 92% chondrules (e.g. Weisberg et al., 2006; Metzler, 2012), i.e., once molten silicate spherules with sizes mostly between 0.1 and 1 millimeter. Further components are metal and sulfide grains, refractory objects like Ca-Al-rich inclusions and amoeboid olivine aggregates (CAIs, AOAs; e.g. Krot, 2019) and fine-grained interchondrule matrix. These components occur in variable and often characteristic amounts in the distinct chondrite groups (e.g. Weisberg et al., 2006). Beside the Rumuruti (R) and Kakangari (K) groups, chondrites are subdivided into three classes, namely the ordinary, enstatite, and carbonaceous chondrites. The latter class consists of nine groups, namely the CI, CY (King et al., 2019), CM, CO, CV, CK, CR, CH, and CB chondrites. Of these, the CI group is particularly distinctive, as these meteorites do not contain any recognizable chondrules and because their bulk chemistry agrees closely with that of the solar photosphere (e.g. Lodders, 2003; Lodders et al., 2009). Each chondrite group is thought to represent a single parent body (or several related parent bodies; e.g., Gattacceca et al., 2020), and so the presence of different groups allows investigating the accretion and early evolution of several distinct primitive planetesimals. As such, identification of a new chondrite group is important for understanding the diversity of planetesimals formed in the early solar system, and the processes that led to this diversity.

In addition to the established carbonaceous chondrite groups there are also ungrouped carbonaceous chondrites, which cannot be assigned to one of these groups. Based on similar properties some ungrouped chondrites can be combined into grouplets (consisting of less than 5 individual members), as in the case of Coolidge and Loongana 001 (Kallemeyn and Rubin, 1995). Coolidge is a well-studied meteorite which was originally classified as a CV4 chondrite (Van Schmus, 1969). However, McSween (1977a) concludes that it cannot simply be a metamorphosed sample of a reduced CV chondrite. By contrast, Kallemeyn and Wasson (1982) concludes that Coolidge represents a CV chondrite, which “was probably subjected to open-system metamorphic reheating”, a conclusion also reached by Scott and Taylor (1985). However, Kallemeyn (1987) subsequently argued that the strong depletion of volatile elements more likely reflects nebular processes and that this meteorite, therefore, may not be a CV chondrite. Further, Noguchi (1994) found that, compared to the reduced CV chondrite Efremovka, chondrules and matrix in Coolidge are systematically depleted in Na, which also points to a nebular rather than a metamorphic process. Finally, based on petrographic observations and characteristic differences in the inventories of volatile elements, Kallemeyn and Rubin (1995) demonstrated that Coolidge clearly does not belong to the CV group, but together with the newly discovered meteorite Loongana 001, defines a new carbonaceous chondrite grouplet.

This study will show that the three ungrouped carbonaceous chondrites Los Vientos (LoV) 051, Northwest Africa (NWA) 033 and NWA 13400 have similar properties as the Coolidge-Loongana 001 grouplet. This makes it possible to combine these five samples into a new carbonaceous chondrite group, which we term the Loongana (CL) group and we define the basic criteria for identifying further members of this group. Since the investigated chondrites have some similarities to CV_{red} chondrites (e.g., McSween 1977a; Gattacceca et al., 2020) and CR chondrites (e.g., Kallemeyn et al., 1994), our

84 discussion concentrates on these groups when comparing petrographic, chemical and isotopic data of
85 CL chondrites.

86

87

2. SAMPLES

88

89 Five ungrouped carbonaceous chondrite finds, namely Coolidge (USA, found 1937), Loongana 001
90 (Australia, found 1990), LoV 051 (Chile, found 2010), NWA 033 (Northwest Africa, found 1999), and
91 NWA 13400 (Northwest Africa, found 2016) are investigated in this study. Polished thin sections
92 (PTS), polished epoxy mounts and polished massive samples (slices) of these chondrites were used
93 for petrographic and microchemical characterization. Subsample designations and masses of
94 analyzed material are given in [Table 1](#). To assess data quality and accuracy, representative bulk
95 powder samples of the Allende CV3 chondrite were analyzed together with those of the above
96 specimens. For comparison, we also determined the matrix fraction of Allende (CV3_{oxA}), Vigarano
97 (CV3_{red}), and NWA 7020 (CR2) as well as the chondrule size-frequency distributions in Allende and
98 NWA 7020.

99 In the following, the meteorite Loongana 001 is termed Loongana for short and we collectively refer
100 to the five investigated meteorites as “CL chondrites” and “CL samples”. The reasoning for naming the
101 proposed new group “CL” is given in section 5.3.1.

102

103

3. METHODS

104

105 All subsamples, including those that were subsequently powdered, were investigated and
106 documented by optical and scanning electron microscopy. Samples of each meteorite were powdered
107 in an agate mortar for obtaining the bulk chemical and isotopic compositions by various techniques.
108 Aliquots for all laboratories, with the exception of LA-ICP-MS (Sc, Se, Te), were taken from the same
109 sample powder ([Table 1](#)). All chemical data are given in wt.% or ppm ($\mu\text{g/g}$), respectively.

110

3.1 Polarizing microscopy

112

113 Polished thin sections (PTS) of all samples were used to determine shock stages and weathering
114 grades by polarizing microscopy. Shock stages were determined according to the instructions given in
115 Stöffler et al. (2018); weathering grades have been determined according to Wlotzka (1993). The latter
116 method was initially developed to characterize ordinary chondrites, but we adopt it here for the use in
117 cases of metal-rich carbonaceous chondrites.

118

3.2 Scanning electron microscopy (SEM)

120

121 The scanning electron microscope (SEM; Jeol JSM-6610LV) of the Interdisciplinary Centre for
122 Electron Microscopy and Microanalysis (ICEM; University of Münster) was used to characterize the
123 sample textures and to identify mineral phases. All subsamples, including slices for subsequent
124 destructive chemical analysis, were documented by preparing photomosaics (backscatter electron

125 images; BSE) of their polished surfaces. BSE images were also used to identify the various meteorite
126 components (chondrules, CAIs, amoeboid olivine aggregates (AOAs), inter-chondrule matrix) and to
127 determine modal abundances and apparent chondrule sizes. For element mapping we used the SEM
128 (Zeiss Sigma 300 VP) at the Institut für Geologie und Mineralogie, University of Cologne.

129

130 *3.2.1 Energy-dispersive X-ray (EDX) analysis*

131 Mineral analyses were obtained using an energy-dispersive X-ray (EDX) analyzing system (INCA,
132 Oxford Instruments); all data were automatically normalized to 100 wt.%. Samples and appropriate
133 mineral standards were measured at a working distance of 10 mm and an acceleration voltage of 20
134 KV. The beam current constancy was controlled by a Faraday cup. The standard ZAF correction
135 procedures were applied (Bence and Albee, 1968). Minerals of known composition (olivine, low-Ca
136 pyroxene and plagioclase from the L6 chondrite Leede; Feldstein et al., 2001) were measured
137 repeatedly as reference materials to ensure the reproducibility of the EDX system. All mineral
138 analyses were checked for stoichiometry. Since none of the chosen analysis methods in this study
139 was able to measure the bulk chondrite S content of the samples, the following procedure was used to
140 obtain a rough estimate of bulk S concentrations. By using the lowest possible magnification (30x) and
141 a duration of 40 seconds each, EDX analyses of 2-3 different PTS regions of each CL sample and
142 Allende were recorded and averaged. The mean S concentration for Allende, obtained by this method,
143 is 1.67 wt.%, compared to the literature value of 2.10 wt.% (Jarosewich et al., 1987). The obtained
144 values for S concentrations in the other samples were multiplied by the resulting correction factor of
145 1.26.

146

147 *3.2.2 Element mapping (phase maps)*

148 We performed element mapping in order to produce phase maps of entire chondrite sections. For
149 this application, the electron beam scanned the stationary sample surface over small areas (~500x400
150 μm , pixel size ~4 μm) with a dwell time of 10 ms per pixel. The accelerating voltage was set to 20 kV
151 and the aperture diameter to 60 μm . The sample was then moved to a new center and the next map
152 was rastered. The phase maps were then produced with the PHAPS application (e.g., Fig. 1; Hezel,
153 2010). These display every mineral phase in false color and allow their visual identification. We further
154 used the phase maps and the software "Measure" (Datinf GmbH, Tübingen, Germany) to determine
155 the modal abundances of CAIs.

156

157 *3.2.3 Determination of apparent (2D) chondrule sizes*

158 The first author of this publication determined the distributions of apparent (2D) chondrule sizes in
159 the five CL chondrites plus those in Allende (CV3_{oxA}) and NWA 7020 (CR2) for comparison. For this
160 purpose the software "Measure" (Datinf GmbH, Tübingen, Germany) was used, stringently following a
161 raster on the BSE photomosaics to not overlook any chondrule cut face. Apparent chondrule sizes
162 were obtained by measuring the diameters of chondrule cut faces at an angle of 45° from the line of
163 the maximum apparent diameter, and thereby a reasonable average between minimum and
164 maximum. It was calculated by Eisenhour (1996) that this method provides a good approximation
165 (within 2%) of the diameter of a circle equal in area to that of the measured ellipse. Except for metal

166 grains, sulfide grains, and CAIs, every subrounded, more or less isometric (aspect ratio $< \sim 2$) object
167 was considered as a chondrule. Chondrules consisting of welded smaller chondrules were measured
168 as one single chondrule. The same holds for chondrules with adhering layers of smaller chondrules
169 and for the rare chondrules with igneous rims. Chondrule fragments with angular fracture surfaces
170 were only included when their original outline could be unequivocally reconstructed (\sim half chondrules).
171 Other chondrule fragments and angular monomineralic grains were omitted. It cannot be ruled out that
172 the data sets contain small fractions of unrecognized roundish chondrule fragments, especially in the
173 smallest size bins ($< 300 \mu\text{m}$).

174

175 **3.3 Electron microprobe (EMPA)**

176

177 The electron microprobe (JEOL 8900RL) at the Institut für Geologie und Mineralogie (University of
178 Cologne) was used for chemical analysis. Mineral compositions (olivine, low-Ca pyroxene, Ca-rich
179 pyroxene) were determined by spot analyses using a focused, stationary beam of $1 \mu\text{m}$, an
180 accelerating voltage of 20 kV, and a beam current of 20 nA. For the analyses of inter-chondrule matrix,
181 the beam was defocused to $30 \mu\text{m}$ and the accelerating voltage was set to 15 kV. The ZAF-algorithm
182 was used for correction (Bence and Albee, 1968). Mineral analyses with totals between 98.5 and
183 101.5 wt.% were accepted.

184

185 **3.4 X-ray fluorescence (XRF)**

186

187 The sample preparation method initially developed by Wolf and Palme (2001) and later modified as
188 described in Stracke et al. (2012) has been used, with a few additional, minor modifications. A sample
189 to standard ratio of 1:30 was used, with typically 120 mg sample material mixed with 3.6 g lithium
190 tetraborate ($\text{Li}_2\text{B}_4\text{O}_7$) flux agent. Before mixing, the sample was pre-treated with aqua regia for a few
191 hours at $120 \text{ }^\circ\text{C}$ to oxidize the metals. A Claisse LeNeo fluxer was used to automatically produce 27
192 mm diameter glass disks. The Panalytical Zetium sequential wavelength dispersive X-ray
193 spectrometer at the University of Cologne was used for sample measurements. Standard calibration
194 lines were calculated from 7 identically prepared standard rock samples. The precision for all elements
195 analyzed is below 1% (Wolf and Palme, 2001). An Allende glass disk was produced and measured in
196 the same way as the samples. The obtained data for Allende are in excellent agreement with literature
197 data. Some CL samples showed low totals which most likely resulted from loss of sample material (~ 2
198 mg, estimated) during sample preparation as well as loss of material during sample fluxing. The latter
199 was possibly caused by the decomposition of weathering products (hydroxides, calcite) and loss of
200 volatile components (H_2O , CO_2). There was only enough powder to determine the loss on ignition
201 (LOI) of NWA 13400 (2.76%, when 120 mg are heated at 1000°C for 2h). This LOI equals ~ 3 mg loss
202 of sample material. We recalculated samples with low totals considering an estimated total loss of
203 material of 5 mg. However, some totals are still low, possibly indicating an underestimation of material
204 loss.

205

206

207 3.5 Trace element compositions

208

209 Trace element concentrations were analyzed on aliquots of the investigated meteorites and an
210 Allende Standard powder (Allende MS-A) for Li, V, Co, Rb, Sr, Y, Zr, Nb, Mo, Cs, Ba, the REE, Hf, Ta,
211 Ti, Pb, Th, and U by isotope dilution sector field inductively coupled plasma mass spectrometry (ID-SF-
212 ICP-MS), as described in detail in Stracke et al. (2012).

213 Concentrations of Sc, Se, and Te in the samples and Allende as a reference material were
214 analysed by LA-ICP-MS at the University of Münster (Institut für Mineralogie). Sample ablation along
215 linear tracks (50 mm each) across the polished sample surfaces (thin and thick sections) was done
216 using 193 nm ArF excimer laser (Analyte G2, Photon Machines). A repetition rate of 10 Hz and an
217 energy of ~ 3-4 J/cm² were used throughout the entire session. The beam spot diameter varied
218 between 80 and 100 µm. Elemental analysis has been carried out with an Element 2 mass
219 spectrometer (ThermoFisher). Forward power was 1300 W and reflected power < 2 W, gas flow rates
220 were 1.2 l/m for He (carrier gas of ablated material), 0.8 l/m and 1.1 l/m for the Ar-auxiliary and sample
221 gas, respectively. Cooling gas flow rate was set to 16 l/min. Before starting analysis, the system has
222 been tuned (torch position, lenses, gas flows) on a NIST 612 glass measuring ¹³⁹La, ²³²Th and
223 ²³²Th¹⁶O to get stable signals and high sensitivity, as well as low oxide rates (²³²Th¹⁶O/²³²Th < 0.1%)
224 during ablation. The above elements were quantitatively analysed using the NIST 612 glass as an
225 external standard and ⁴³Ca as internal standard; Ca concentrations had been previously determined
226 by XRF. Concentrations of measured elements were calculated using the Glitter software (Griffin et al.,
227 2008). Standard reference glasses GSD1-G and GSE1-G were analysed as monitor for precision and
228 accuracy. Obtained results match the published range of concentrations given in the GeoReM
229 database (version 24; Jochum et al., 2005).

230

231 3.6 Titanium and chromium isotopes

232

233 Aliquots of ~35 mg sample powder (equivalent to ~20-30 µg Ti) were digested in HF-HNO₃-HClO₄
234 (2:1:0.05) on a hotplate at 180–200 °C for five days and in aqua regia (HCl-HNO₃) at 130–150 °C for
235 another two days. Thereafter, the samples were dissolved in 12 M HNO₃, and ~65 mg H₃BO₃ was
236 added. Ti was separated from the sample matrix via a two-stage anion exchange chromatography
237 adapted from the previously established procedure from Zhang et al. (2011). In a first step, the sample
238 solutions were loaded onto columns prepacked with 2 ml TOGDA® anion exchange resin, where Ti
239 was eluted in 20 ml 12 M HNO₃–1 wt.% H₂O₂. Afterwards, the Ti cuts were dissolved in 2.5 ml 4 M HF
240 and loaded onto clean-up columns filled with 0.8 ml Bio-Rad® AG1-X8 anion exchange resin, where Ti
241 was eluted in 6 ml 9 M HCl–0.01 M HF.

242 Titanium isotope measurements were performed in two lines using a ThermoScientific Neptune
243 Plus MC-ICP-MS (Institut für Planetologie, University of Münster) in medium resolving power mode
244 (Zhang et al., 2011). Solutions containing about 200 ppb Ti in 0.3 M HNO₃–0.0014 M HF were
245 introduced through a Cetac Aridus II desolvating system, resulting in a ~3.5×10⁻¹⁰ A ion beam on ⁴⁸Ti.
246 Measurements consisted of a 30 s baseline measurement (deflected beam) followed by 40 isotope
247 ratio measurements of 4.2 s each. Mass bias was corrected using the exponential law and ⁴⁹Ti/⁴⁷Ti =

248 0.749766. The Ti isotope anomalies are reported as parts per ten thousand deviation (ϵ -notation) from
249 the terrestrial OL-Ti (Millet and Dauphas, 2014) bracketing standard. The sample uncertainty is
250 reported as the Student-t 95% confidence interval based on repeated analyzes (N=12) of the sample
251 solution.

252 Chromium was collected during the first step of the two-stage anion exchange chromatography
253 used for the separation of Ti, where Cr is eluted in 25 ml 12 M HNO₃ (+ trace H₃BO₃) together with
254 most other matrix elements. Aliquots (equivalent to ~30 μ g Cr) were taken from this solution, dried
255 down, and redissolved in 1 ml 6 M HCl. Afterwards, Cr was separated from the sample matrix using a
256 single-stage anion exchange chemistry for the removal of Fe (Bio-Rad® AG1-X8 anion exchange
257 resin), followed by a two-stage cation exchange chromatography (Bio-Rad® AG50W-X8 cation
258 exchange resin) as described by Yamakawa et al. (2009), including a four-day conversion of
259 Cr[III]Cl₃/Cr[II]Cl₂ to Cr³⁺.

260 Chromium isotope measurements were performed using a ThermoScientific Triton Plus Thermal
261 Ionization Mass Spectrometer (Institut für Planetologie, University of Münster) in static mode. The
262 sample solutions (containing ~500 ppm Cr in 6 M HCl) were loaded on 4-6 filaments and each filament
263 was measured multiple times, with total ion beam intensities of ~1.4×10⁻¹⁰ A on ⁵²Cr. Instrumental
264 mass fractionation was corrected assuming a constant ⁵⁰Cr/⁵²Cr = 0.051859 and using the exponential
265 law. The data are reported in $\epsilon^{54}\text{Cr}$ values as the parts per ten thousand deviation from the terrestrial
266 NIST SRM3112a Cr standard. The sample uncertainty is reported as the Student-t 95% confidence
267 interval based on repeated analyses (N=8-12).

268

269 3.7 Oxygen isotopes

270

271 Oxygen isotope analyses were obtained at the Open University using an infrared laser-assisted
272 fluorination system (Miller et al., 1999; Greenwood et al., 2017). Samples and standards were weighed
273 out into a Ni sample block with each aliquot having a mass of approximately 2 mg. The block was
274 loaded into a vacuum-tight chamber and heated to 70°C under vacuum overnight to remove surface-
275 bound moisture. The system was then flushed with BrF₅ to reduce the final blank level to <60 nmoles
276 O₂. Oxygen was released from the samples by heating in the presence of BrF₅ using a 50 W infrared
277 CO₂ laser. After fluorination, the released oxygen gas was purified by passing it through two cryogenic
278 nitrogen traps and over a bed of heated KBr to remove any excess fluorine. Oxygen gas was analyzed
279 using a MAT 253 dual inlet mass spectrometer. Overall system precision, as defined by replicate
280 analyses of our internal obsidian standard is: $\pm 0.053\text{‰}$ for $\delta^{17}\text{O}$; $\pm 0.095\text{‰}$ for $\delta^{18}\text{O}$; $\pm 0.018\text{‰}$ for $\Delta^{17}\text{O}$
281 (2σ) (Starkey et al., 2016).

282 Oxygen isotopic analyses are reported in standard δ notation, where $\delta^{18}\text{O}$ has been calculated as:
283 $\delta^{18}\text{O} = [({}^{18}\text{O}/{}^{16}\text{O})_{\text{sample}}/({}^{18}\text{O}/{}^{16}\text{O})_{\text{VSMOW}} - 1] \times 1000$ (‰) and similarly for $\delta^{17}\text{O}$ using the ${}^{17}\text{O}/{}^{16}\text{O}$ ratio.
284 $\Delta^{17}\text{O}$, which represents the deviation from the terrestrial fractionation has been calculated as $\Delta^{17}\text{O} =$
285 $\delta^{17}\text{O} - 0.52 \delta^{18}\text{O}$.

286

287

288

289 **3.8 Magnetic measurements**

290

291 All magnetic measurements were performed at CEREGE (Aix-en-Provence, France). Hysteresis
292 measurements were performed with a Princeton Micromag Vibrating Sample Magnetometer (VSM)
293 with a maximum applied field of 1 T and a sensitivity of $\sim 5 \times 10^{-9}$ Am². The analysis of hysteresis loops
294 provided the ratio of saturation remanent magnetization (M_{RS}) to saturation magnetization (M_S) and the
295 coercive force (B_C). High field susceptibility (χ_{HF}) was determined by a linear fit for applied fields > 0.9
296 T of the hysteresis loops. Remanent coercive force (B_{CR}) was determined by back field experiments
297 performed with the VSM. The low field specific susceptibility (χ in m³/kg) was measured using Agico
298 MFK1 apparatus with sensitivity of 5×10^{-13} m³, operating at 200 A/m and a frequency of 976 Hz. We
299 determined the S-300 ratio, defined as the isothermal remanent magnetization (IRM) obtained after
300 applying a 3 T field and then a back field of 0.3 T normalized to the IRM acquired in 3 T. For this
301 experiment, IRM were imparted using a pulse magnetizer from Magnetic Measurement.

302

303

303 **4. RESULTS**

304

305 **4.1 Meteorite textures**

306

307 The investigated samples are mainly composed of the typical carbonaceous chondrite
308 components, namely type I chondrules, refractory inclusions (CAIs, AOAs), some inter-chondrule
309 sulfide and metal grains and a fine-grained inter-chondrule matrix. Cut faces of the least weathered
310 sample (LoV 051) show well-preserved tiny metal beads within and at the periphery of chondrules.
311 Occasionally, large fragments of chondrules and refractory inclusions occur, but all samples are
312 macroscopically unbrecciated. Their overall textures show some resemblance to the reduced CV
313 chondrites (CV_{red}) and CR chondrites, but differ in having a very low amount of inter-chondrule matrix
314 (see section 4.7.3) and consequently a relatively high chondrule content. The compositions and
315 textures of Coolidge and Loongana have been described by Noguchi (1994) and Kallemeyn and Rubin
316 (1995). The overall texture of Loongana is shown in Fig. 1 both as a photomosaic of SEM-BSE images
317 (a) and a phase map (b). The following components can be distinguished in Fig. 1: abundant
318 porphyritic (1,6) and rare non-porphyritic chondrules (2), rare Al-rich chondrules (3), chondrule
319 fragments (4), adhering chondrules (5), olivine chondrules (6) with thick pyroxene rims (7), and CAIs
320 (8). These components are described in detail below (section 4.7).

321

322 **4.2 Petrologic types**

323

324 Coolidge and Loongana are listed as being C4-ungrouped in the Meteoritical Bulletin Database
325 (MBDB). However, they have also been classified as type 3.8 to 4 and type 3.8 by Kallemeyn and
326 Rubin (1995) and Guimon et al. (1995). The samples NWA 033 and LoV 051 are listed as C3-
327 ungrouped in the MBDB, without allocation to a certain petrologic subtype. NWA 13400 is listed as C3-
328 ungrouped, with a proposed petrologic subtype of 3.9. One of the standard methods to identify a
329 chondrite's subtype is determining the frequency distribution of fayalite (Fa) values of randomly

330 chosen olivine grains. The percentage mean deviation (PMD) of these values is used as a measure for
331 the equilibration state of a given meteorite (e.g. Hutchison, 2004; his Table 2.6). We determined these
332 distributions in all samples, together with the frequency distributions of ferrosilite (Fs) values of their
333 low-Ca pyroxene grains; the results are shown in Fig. 2. Occasionally, chondrules and chondrule
334 fragments with relict Mg-rich core compositions of olivine can be found in all samples. The PMD
335 values for Coolidge, Loongana, and NWA 033 are below 5% (Table 2), indicating that these samples
336 belong to petrologic type 4, whereas those of LoV 051 and NWA 13400 are between 5% and 10%,
337 indicating a 3.9 subtype.

338

339 4.3 Shock stages

340

341 All olivine grains in the investigated CL chondrites show undulatory extinction, but grains with
342 planar fractures are rare or absent. Thus, all these samples are weakly shocked (Table 2) and belong
343 to shock stage C-S2 (Stöffler et al., 2018), corresponding to the previously defined shock stage S2
344 (Stöffler et al., 1991).

345

346 4.4 Weathering grades

347

348 Most samples are moderately to heavily weathered (W2-W3/4) and crosscut by veins composed of
349 the secondary alteration products of metals and sulfides. Nevertheless, variable amounts of Fe-Ni
350 metal are still visible on cut faces of all samples. The estimated degrees of weathering for the CL
351 samples, which were determined using the scheme of Wlotzka (1993), are given in Table 2. The least
352 weathered CL chondrite of this study is LoV 051 (W1/2), which still contains considerable amounts of
353 pristine metal.

354

355 4.5 Magnetic properties

356

357 The magnetic properties of four CL chondrites from this study are given in Table 3, together with
358 data for the various CV subgroups (CV_{red} , CV_{oxA} , CV_{oxB}) and CR chondrites for comparison. The
359 magnetic properties of all samples, with the notable exception of LoV 051, have been considerably
360 modified by terrestrial weathering. Thus, the data for LoV 051 are the most relevant for defining the
361 primary characteristics of the proposed CL group. Its magnetic susceptibility (Table 3) is $\log \chi = 5.24$
362 (where χ is in $10^{-9} \text{ m}^3 \text{ kg}^{-1}$), higher than the corresponding values for Coolidge, Loongana, and NWA
363 033. This difference can be accounted for by terrestrial weathering, which lowers the susceptibility of
364 metal-bearing meteorites (Rochette et al., 2008). The susceptibility of LoV 051 ($\log \chi = 5.24$) is slightly
365 higher compared to CR chondrites, which have an average $\log \chi = 5.04 \pm 0.12$ as measured on 14 CR
366 meteorites (Rochette et al., 2008), and almost identical to the value for the only CR chondrite fall
367 Renazzo ($\log \chi = 5.17$). The observed hysteresis loop for LoV 051 is typical of kamacite-bearing rocks
368 (Gattacceca et al., 2014), including a curvature up to above 700 mT, very low coercivity ($B_C = 3.08 \text{ mT}$),
369 very low M_{RS}/M_S ratio (0.0155), and high B_{CR}/B_C ratio (6.10). Together with the S_{300} value of 1.00,
370 there is strong evidence that the magnetic mineralogy is dominated by kamacite.

371

372 4.6 Modal compositions

373

374 The modal compositions of all samples, as well as Allende ($CV_{3_{oxA}}$) and Vigarao (CV_{red}) for
375 comparison, were obtained by point counting on SEM-BSE images. The results for the CL chondrites
376 are summarized in Table 2. The modal abundances (area% = vol%) of chondrules and chondrule
377 fragments in our samples vary between 67 vol% (Loongana) and 79 vol% (Coolidge). The inter-
378 chondrule metal and sulfide concentration, modified by terrestrial weathering, varies between 3 vol%
379 (Coolidge) and 6 vol% (NWA 033, NWA 13400; Table 2). The concentration of CAIs, measured on
380 phase maps (e.g., Fig. 1), appears highly variable (from 0.1 vol% for Coolidge to 8 vol% for
381 Loongana). For the modal abundance of inter-chondrule matrix we obtained values between 17 vol%
382 (LoV 051, NWA 13400) and 21 vol% (NWA 033; Table 2).

383 To verify our method, we also determined the abundances of matrix in Allende (CV_{oxA}) and
384 Vigarano (CV_{red}) and found values of 46 vol% and 35 vol%, respectively. The value for Allende is in
385 the range of values obtained by McSween (1977a; 38.4 vol%) and Gattacceca et al. (2020; 50 vol%).
386 Our Vigarano value is nearly identical to that of McSween (1977a; 34.5 vol%) and identical to that
387 given in Gattacceca et al. (2020). Thus, our method reproduces literature values well, demonstrating
388 that CL chondrites contain significantly less matrix than CV chondrites and most other carbonaceous
389 chondrites.

390

391 4.7 Lithologic components

392

393 4.7.1 Chondrules

394 The investigated CL chondrites consist mainly of chondrules (67-79 vol%; Table 2), including minor
395 amounts of chondrule fragments. In the following the term “chondrules” also includes chondrule
396 fragments, if not stated otherwise.

397

398 4.7.1.1 Chondrule textures, types, and mineralogical compositions

399 Chondrules in the investigated meteorites are mostly porphyritic olivine (PO) and porphyritic
400 olivine-pyroxene (POP) chondrules of chemical type I. A high percentage of these show pyroxene rims
401 (see section 4.7.1.3). Many of these have non-circular, irregular boundaries, which has already been
402 described for Coolidge and Loongana by Kallemeyn and Rubin (1995). Many chondrules in our
403 samples, especially the smaller ones, give the impression of rapidly crystallized droplets from
404 fragmented or shredded melts, which partly accumulated in a viscous state. They show remarkably
405 irregular shapes with lobate outlines and protuberances (Fig. 3a) and sometimes display an
406 amoeboidal shape (Fig. 3b). In some cases it is difficult to define the outlines and boundaries between
407 adjacent objects (Fig. 3c). Many chondrules are the result of adhesive growth from smaller chondrules,
408 i.e. they are part of welded chondrule agglomerates or adhere to the surface of larger chondrules.
409 They form irregular layers of smaller roundish chondrules stacked on top of each other. A striking
410 example is shown in Fig. 3d (white outline), which appears to be an agglomeration of small chondrules
411 and lobate melt droplets around a central chondrule, separated by an Fe-Ni layer (white).

412 Chondrule olivine is nearly equilibrated in most samples (Table 4; Fig. 2a). The lowest Fa values
413 for olivine grains found in this study (beside the rare relict Mg-rich olivine cores) are around 10 mol%.
414 This value is also the arbitrarily defined boundary between the chemical chondrule types I (<10 mol%
415 Fa) and II (McSween, 1977b; Jones et al., 2005; Lauretta et al., 2006). However, the presence of Fe-
416 Ni metal in most chondrules in our samples (Figs. 3a-f) relates them to type I. In case of larger
417 chondrules there is a tendency that metal occurs as outer shells (e.g., Fig. 3g). In several cases, metal
418 forms one or two concentric layers within the chondrules (Figs. 3e-f), which may indicate that these
419 structures formed by agglomeratic growth. The largest Fe-Ni metal grains in chondrules were found in
420 LoV 051 (1.1 mm) and Coolidge (1.6 mm). The metal mainly consists of polycrystalline kamacite with
421 small amounts of taenite exsolutions (Fig. 4a). The Ni concentration in kamacite is fairly constant in all
422 samples, with mean concentrations ranging between 7.1 wt.% (NWA 13400) and 8.0 wt.% (NWA 033).
423 Measured Ni concentrations in taenite are variable, with values between 13.5 wt.% and 41.0 wt.%.
424 This is consistent with the results of Scott and Taylor (1985) and Noguchi (1994) who found mean Ni
425 concentrations of 6.4-7.1 wt.% and 19.2-20.9 wt.% for kamacite and taenite, respectively, in Coolidge.
426 In many kamacite grains, tiny subrounded grains of chromite, merrillite, and SiO₂ occur as exsolutions
427 along internal metal grain boundaries (Fig. 4a). A side-by side occurrence of isolated kamacite and
428 taenite grains in chondrules was only rarely observed (Fig. 4b). Polycrystalline, primary sulfide grains
429 (troilite, FeS) up to 500 μm large and frequently intergrown with kamacite, can also be found in these
430 chondrules (Fig. 4c-d). In some chondrule cut faces the sulfide + metal portion exceeds 50 area%.
431 Some metal grains up to 1 mm in size occur outside of chondrules. Chondrule plagioclase
432 compositions are variable (An₇₂-An₉₉) with negligible K concentrations. Noguchi (1994) found values of
433 An₂₇-An₉₅ in Coolidge. Plagioclase is concentrated in chondrule mesostases, frequently in the shape
434 of lath-like intergrowths with Ca-rich pyroxene.

435 Some Al-rich chondrules have been observed in Loongana (Fig. 3g) and LoV 051, and non-
436 porphyritic chondrules (barred olivine; BO) were found in Coolidge and NWA 13400 (Fig. 3h).

437 In all samples Mg-rich relict olivine cores are found, attesting that type I chondrules were present
438 prior to thermal metamorphism. Occasionally, chondrules of chemical type II can be observed in the
439 samples (e.g. BO chondrule in Fig. 3h) which can be identified by their metal-free composition.

440

441 4.7.1.2 Chemistry of main minerals

442 The chemical compositions of the main mineral phases found in chondrules (olivine, low-Ca
443 pyroxene, and Ca-rich pyroxene) were measured by EMPA. Relict Mg-rich olivine cores are
444 occasionally found in all samples, but were not measured during the random analyses. A number of 30
445 to 49 olivine grains were measured in each sample and the variation of Fa values is shown in Fig. 2a.
446 The mean Fa values (mol%; Table 4) vary between 12.5 (Loongana) and 14.7 (NWA 13400). The Fa
447 values for Coolidge and Loongana (14.5 and 12.5) are similar to those presented in earlier studies.
448 Scott and Taylor (1985) and Noguchi (1994) found Fa values of 14 in Coolidge; Kallemeyn and Rubin
449 (1995) give a value of 13.6. The mean Fa value for Loongana found by the latter is 11.8. The mean
450 FeO/MnO ratios (wt.%/wt.%) in olivine of our samples vary between 52 (Loongana) and 61 (NWA
451 13400). Noguchi (1994) found a mean value of 64 in Coolidge, compared to our value of 60.

452 Between 20 and 49 low-Ca pyroxene grains were measured in each sample and the Fs variation is
453 presented in Fig. 2b. The mean Fs values (mol%; Table 5) vary between 6.6 (NWA 13400) and 10.4
454 (Loongana). Noguchi (1994) and Kallemeyn and Rubin (1995) found mean Fs values of 10.1 and 9.3,
455 respectively, in Coolidge, compared to our value of 9.4. The mean Fs value of 6.9 for Loongana given
456 in Kallemeyn and Rubin (1995) is somewhat lower than our value (10.4), possibly indicating sample
457 inhomogeneity. The mean wollastonite (Wo) values in all samples vary between 0.9 and 1.1 mol%
458 (Table 5). The mean FeO/MnO ratios (wt./wt.%) in low-Ca pyroxene are similar and vary between
459 38 (NWA 13400) and 46 (Coolidge). Low-Ca pyroxene phenocrysts with extremely high Al₂O₃ contents
460 (9-13 wt.%) have been found in a quenched Al-rich chondrule in Loongana (Fig. 3g; dark gray
461 crystals). Similar pyroxene compositions have been found by Noguchi (1994) in a BO chondrule from
462 Coolidge.

463 Ca-rich pyroxene is another major mineral phase in chondrules. Between 8 and 38 grains were
464 measured in each sample and the mean Fs and Wo variations (mol%) are presented in Table 6. The
465 mean Fs values vary between 4.2 (NWA 13400) and 6.6 (Coolidge) and the mean FeO/MnO ratios
466 (wt./wt.%) vary between 13 and 20. The mean Wo values vary between 30.9 (Loongana, NWA
467 13400) and 38.6 (NWA 033; Table 6).

468

469 4.7.1.3 Fractions of chondrules with pyroxene rims

470 Many of the type I PO and POP chondrules, especially the larger ones, are mantled by low-Ca
471 pyroxene layers (Figs. 1, 3e), a typical feature in carbonaceous (and other) chondrites (e.g. Friend et
472 al., 2016; Barosch et al., 2019). We systematically quantified the 2-dimensional fractions of
473 mineralogically zoned chondrules using the produced phase maps. Fractions are lowest in Coolidge
474 (57%), intermediate in LoV 051 (58%), Loongana (59%) and NWA 033 (60%), and highest in NWA
475 13500 (62%). Barosch et al. (2020) demonstrated that 2D studies underestimate the true (3D) zoned
476 chondrule fractions and proposed a 2D-3D correction factor of 1.24 for carbonaceous chondrites. The
477 so calculated average 3D zoned chondrule fraction in the investigated samples is ~73%, a value
478 typical for carbonaceous chondrites (Friend et al., 2016; Barosch et al., 2020).

479

480 4.7.1.4 Apparent chondrule sizes

481 We measured the apparent (2D) chondrule sizes in the five CL chondrites as well as in Allende and
482 the CR2 chondrite NWA 7020 for comparison. Obvious chondrule fragments and angular
483 monomineralic grains were excluded from these measurements (see section 3.2.3). The identification
484 of chondrule outlines were sometimes obfuscated by the complex chondrule textures described in
485 section 4.7.1.1). Our chondrule sizes (diameters) include the irregular layers of adhering smaller
486 chondrules and (rarely observed) igneous rims. The statistics for the size-frequency distributions are
487 given in Table 7. The original size data can be found in the Electronic Annex of this publication. We
488 measured between 145 and 512 chondrules per sample and found a fairly restricted range of mean
489 apparent (2D) chondrule sizes, which are between 404 μm (Coolidge) and 477 μm (NWA 13400).
490 These are similar to that of the CV_{ox} chondrite Allende (470 μm), but considerably smaller than that of
491 the CR chondrite (mean 633 μm; Table 7). The same holds for the values of the median sizes and
492 standard deviations. The measured size-frequency distributions of the investigated CL chondrites are

493 shown in Fig. 5a. In Fig. 5b their mean size distribution is compared to the distributions found in the
494 present study for the CV chondrite Allende and the CR chondrite NWA 7020. The mean CL distribution
495 is similar to that of Allende, but the CR distribution differs in having much larger fractions of large (>
496 600 µm) chondrules and correspondingly lower fractions of smaller chondrules.

497

498 4.7.2 Refractory inclusions (CAIs and AOAs)

499 The largest CAIs found in our study are from NWA 13400 and Loongana, with maximum apparent
500 sizes of 3.8 and 2.8 mm, respectively. The occurrence of CAIs in Loongana and Coolidge has been
501 described by Noguchi (1994) and Kallemeyn and Rubin (1995) with maximum sizes of 500 µm in
502 Coolidge. All CAIs in our samples are fine-grained and consist mainly of an intergrowth of spinel,
503 plagioclase, and Ca-rich pyroxene. Similar CAI textures were also described by Noguchi (1994) for the
504 Coolidge meteorite. A complex CAI in Loongana is shown in Fig. 6a, which consists of fine-grained
505 subunits (anorthite, spinel), rimmed by Ca-rich pyroxene. Some FeS is also present in this CAI.
506 Several other CAIs are rich in FeS, probably a result of secondary alteration on the parent asteroid. An
507 example is shown in Fig. 6b from NWA 13400, which consists of anhedral to euhedral spinel grains,
508 embedded in a fine-grained groundmass of spinel, FeS, and plagioclase. This inclusion is partially
509 rimmed by Ca-rich pyroxene. Spinel grains in all CAIs are zoned, with decreasing Mg- and Al-contents
510 and increasing Cr- and Fe-contents from core to rim. This confirms observations by Noguchi (1994) for
511 Coolidge. In a CAI from this meteorite we found an assemblage of spinel + FeS + TiO₂ (probably rutile;
512 Fig. 6c). This CAI is rimmed by an outer layer of diopside and an inner layer of spinel, possibly
513 remnants of a former Wark-Lovering rim. CAIs in the investigated meteorites are frequently
514 accompanied by large grains of Cl-apatite, either on their edges (up to 500 µm) or in their interiors (up
515 to 100 µm; Fig. 6d). These phosphates possibly formed by the release of large amounts of Ca during
516 alteration of CAIs. This relation was also observed in Coolidge by Noguchi (1994). Moreover, we found
517 a small (7 µm) refractory metal nugget with high concentrations of Os, Ir, Pt, and Ru in a CAI in
518 Loongana, placed within a region of altered Fe-Ni metal (Fig. 6e).

519 Small (< a few hundred µm) amoeboid olivine aggregates (AOAs) were found in Coolidge by
520 Noguchi (1994). We found a large AOA with an apparent maximum size of 900 µm in LoV 051 (Fig.
521 6f), which consists of a porous part rich in olivine and a more compact part that contains small CAI-like
522 units. These units mainly consist of Ca-rich plagioclase (An₇₀) and chromian spinel.

523

524 4.7.3 Inter-chondrule matrix

525 The modal amount of inter-chondrule matrix (termed “matrix” in this section) is low in the
526 investigated samples (17-21 vol%; Table 2). The matrix mainly consists of an assortment of olivine
527 grains with smaller amounts of low-Ca pyroxene and some plagioclase. Similar observations were
528 described by Noguchi (1994) for the Coolidge meteorite. Fe-rich materials fills the pore spaces and
529 probably represent oxidation products of metals and sulfides (Fig. 7a), a conclusion also given in
530 McSween (1977a). The grain size distribution of matrix components is bimodal, where larger grains
531 (~5-30 µm) are embedded in a groundmass of smaller grains with sizes mostly between ~0.2 and ~1
532 µm (Fig. 7b-f). The majority of larger grains represent fragments of larger objects, probably
533 chondrules, with fracture surfaces and irregular outlines. Beside some angular fragments, the smaller

534 grains are a mixture of isometric to slightly elongated grains, which may have crystallized during
535 thermal metamorphism. The mean chemical compositions of matrix in the investigated samples,
536 obtained by EMPA, are listed in [Table 8](#), together with literature data for other carbonaceous chondrite
537 groups. To provide a better comparison with our values, the literature data of McSween and
538 Richardson (1977) in this table have been recalculated to totals of 95%.

539

540 **4.8 Bulk meteorite elemental compositions**

541

542 *4.8.1 Major and minor elements*

543 The measured bulk concentrations of major and minor elements in the CL chondrites and the
544 Allende reference sample are listed in [Table 9](#), together with literature data for Coolidge, Loongana,
545 and Allende. The measured values for Allende are well within or close to the range of literature values.
546 Our FeO (30.99 wt.%) and Na₂O (0.32 wt.%) value for Coolidge appears high compared to literature
547 values (24.83-27.04 and 0.24-0.26 wt.%, respectively). However, our values for FeO and Na₂O of the
548 Allende reference sample are in the range of literature values, thus showing no systematic analytical
549 bias. None of the chosen analysis methods of this study was able to measure the bulk S content of the
550 samples and we used SEM-EDX data to obtain a rough estimate of the S concentrations (see section
551 3.2.1). These results are also included in [Table 9](#).

552 Compared to Allende, the CL chondrites are slightly depleted in Al and K and strongly depleted in
553 Mn and Na. Hence, they are chemically well discriminated from the other groups of carbonaceous
554 chondrites on, e.g., an Al₂O-MnO plot ([Fig. 8a](#)).

555

556 *4.8.2 Trace elements*

557 The measured bulk concentrations of trace elements in the samples and in the Allende reference
558 sample are listed in [Table 10](#), together with literature data for Coolidge, Loongana, and Allende. Our
559 measurements are plotted in [Figs. 8b-c](#) and [Figs. 9-10](#), together with data for major and minor
560 elements. The measured values for Allende are well within or close to the range of literature values
561 ([Table 10](#)). As noted above, severe weathering effects were detected for Loongana and NWA 033. For
562 example, in these meteorites the light rare earth elements (REEs) were enriched during terrestrial
563 weathering, a process described by, e.g., Pourkhorsandi et al. (2017a). These data and some for the
564 other samples are shown in italics in [Table 10](#) and are neither included in the figures nor will they be
565 included in the discussion.

566 Only few literature data exist on the chemical composition of Coolidge (Kallemeyn and Rubin,
567 1995; Weckwerth, 2014; [Table 10](#)). Compared to these, our values for Sc and Se are higher and those
568 for V and Hf are somewhat lower ([Table 10](#)). Compared to literature data (Kallemeyn and Rubin,
569 1995), our Loongana value for Se is somewhat higher and those for V and Zn are somewhat lower.
570 Again, since our values for the respective elements in the Allende reference sample are in the range of
571 literature data, there is no systematic analytical bias. The investigated CL chondrites are chemically
572 well discernable from the other carbonaceous chondrite groups on Al₂O₃ vs. Zn ([Fig. 8b](#)) and Zr vs. Rb
573 ([Fig. 8c](#)) plots, which reveal the typical depletion of volatile elements such as Rb and Zn.

574

575

576 **4.9 Bulk meteorite isotope compositions**

577

578 *4.9.1 Oxygen isotopes*

579 The measured values for $\delta^{17}\text{O}$, $\delta^{18}\text{O}$, and $\Delta^{17}\text{O}$ of the investigated CL chondrites and Allende are
580 listed in [Table 11](#) and plotted in [Fig. 11](#). The compositional fields for CR, CV3, CK, and CO3
581 chondrites are shown for comparison. All CL samples plot along the Carbonaceous Chondrite
582 Anhydrous Mineral (CCAM) line (Clayton and Mayeda, 1999) with $\Delta^{17}\text{O}$ values between -3.96 and -
583 5.47‰. The CL data plot either directly on this line (NWA 033, NWA 13400) or slightly off it and in the
584 direction of the Primitive Chondrule Minerals (PCM) line (Ushikubo et al., 2011). Three of the CL
585 samples (Loongana, NWA 033, NWA 13400) plot within the range of CV3 and CK chondrites, while
586 Coolidge and LoV 051 have considerably lower $^{17}\text{O}/^{16}\text{O}$ and $^{18}\text{O}/^{16}\text{O}$ ratios.

587

588 *4.9.2 Titanium and chromium isotopes*

589 The Ti and Cr isotopic data are provided in [Table 12](#) and visualized in [Fig. 12](#). In [Fig. 12a](#) the $\epsilon^{54}\text{Cr}$
590 data are plotted vs. the corresponding $\Delta^{17}\text{O}$ values and in [Fig. 12b](#) the $\epsilon^{54}\text{Cr}$ values are plotted vs. the
591 $\epsilon^{50}\text{Ti}$ data. In such diagrams the dichotomy between non-carbonaceous and carbonaceous chondrites
592 is strikingly evident (Warren, 2011; Kleine et al., 2020). Although the $\epsilon^{54}\text{Cr}$ values of the five CL
593 chondrites are similar to the mean compositions of CO and CV chondrites ([Fig. 12a](#)), the CL
594 chondrites plot in a distinctly different region of the $\epsilon^{54}\text{Cr}$ - $\epsilon^{50}\text{Ti}$ diagram, where they do not overlap with
595 the compositions of CO and CV chondrites ([Fig. 12b](#)). Instead, in terms of $\epsilon^{50}\text{Ti}$ the CL chondrites are
596 more similar to CM and CR chondrites. All CL chondrites have indistinguishable $\epsilon^{50}\text{Ti}$ and $\epsilon^{54}\text{Cr}$ values,
597 and so the mean Ti and Cr isotope composition of the CL group can be precisely defined from these
598 data. This in turn makes it possible to use these data for evaluating the genetic relationship of CL
599 chondrites relative to other carbonaceous chondrite groups.

600

601

601 **5. DISCUSSION**

602

603 **5.1 Characteristics of CL chondrites and differences to other chondrite groups**

604

605 The investigated samples share many textural, chemical, and isotopic properties. Macroscopically
606 they remotely resemble CV_{red} and CR chondrites, but there are many differences to these and other
607 carbonaceous chondrite groups, as discussed in the following.

608

609 *5.1.1 Chondrules*

610 Most chondrules are PO and POP varieties of petrologic type I, rich in Fe-Ni metal. Many small
611 chondrules show a remarkably irregular outer shape with lobate outlines and protuberances ([Fig. 3a](#))
612 or even have an amoeboidal shape ([Figs. 3b,c](#)). Many of the small chondrules are concentrated in
613 layers around larger chondrules ([Fig. 3d](#)). However, such textures are not unique to these samples,
614 but were occasionally observed by us in the CV_{red} chondrite Vigarano and the CR chondrite NWA
615 7020, as well. A distinctive feature of the CL samples is their high chondrule abundance (67 to 79

616 vol%; [Table 2](#)). Kallemeyn and Rubin (1995) found nearly the same chondrule abundance in
617 Loongana (~70% vs. 67% in this study), but a lower abundance in Coolidge (60-65% vs. 79% in this
618 study), possibly reflecting sample heterogeneity. McSween et al. (1977a) found 67 vol% chondrules in
619 Coolidge. For comparison, chondrule concentrations in CV and CR chondrites are 45% and 50-60%,
620 respectively (Krot et al, 2014), i.e. considerably lower than in CL chondrites.

621

622 *5.1.2 Apparent chondrule sizes*

623 The observed range of mean apparent chondrule sizes in the CL samples is restricted to values
624 between 404 and 477 μm ([Table 7](#)). To verify our method, we also measured the apparent (2D)
625 chondrule sizes in the CR2 chondrite NWA 7020 and the CV chondrite Allende ([Table 7](#); [Fig. 5b](#)). It is
626 found that the CL values of mean chondrule sizes overlap with those in the CV chondrite Allende
627 (CV_{oxA} ; 470 μm ; [Table 7](#)). Other statistical parameters of the CL chondrites size-frequency
628 distributions (median size, standard deviation, and skewness) are also similar to those displayed by
629 Allende ([Table 7](#)), hinting at a possible relationship to CV chondrites. The mean sizes are distinctly
630 smaller than the 633 μm found in the CR chondrite NWA 7020 ([Tab. 7](#)). Literature values of mean
631 apparent chondrule sizes for Coolidge and Loongana (610 μm and 700 μm ; Kallemeyn and Rubin,
632 1995) are larger than those found by us (404 μm and 414 μm). The likely explanation is that we
633 measured a large number of chondrules (145 and 235; [Table 7](#)) on BSE photomosaics, whereas the
634 literature values were obtained from only 23-52 chondrules (Kallemeyn and Rubin 1995) using optical
635 microscopy. This could have led to an overrepresentation of large chondrules in their statistics.

636 Our mean value for the CR2 chondrite (633 μm) is in the range of published values for five other
637 CR chondrites (490-770 μm) and close to the corresponding average value (658 μm ; Kallemeyn et al.,
638 1994). In case of Allende a verification of our mean value (470 μm) is more complicated since
639 literature data vary considerably, with mean values of 915 μm (Teitler et al., 2010), 765 μm
640 (Gattacceca et al., 2020), and 310 μm (Simon et al., 2018). Sample inhomogeneity may be partly
641 responsible for these variations. Furthermore, the different methods of investigation certainly
642 contribute to these differences, i.e., chondrule separation (true chondrule sizes; Teitler et al., 2010),
643 optical microscopy (apparent chondrule sizes; Gattacceca et al., 2020), and scanning electron
644 microscopy (apparent chondrule sizes; x-ray compositional images, Simon et al., 2018; BSE images,
645 this work). Furthermore, the classification of small subrounded particle cut faces as chondrules or
646 fragments is a source of subjective bias.

647 From the presented results it can be concluded that the chondrule-size-frequency distributions and
648 mean chondrule sizes in CL chondrites are similar to each other and to those in CV chondrites, but
649 dissimilar to those in CR chondrites ([Fig. 5](#); [Table 7](#)).

650

651 *5.1.3 Mean olivine compositions*

652 Similar mean compositions of olivine (Fa 12.5-14.7 mol%; [Table 4](#)) are a further distinctive feature
653 of CL chondrites. However, this property is of secondary origin, established by thermal metamorphism
654 on the parent body. This cannot not be a criterion for recognizing unequilibrated CL samples that may
655 be identified in the future (see section 5.3.3). On the other hand, this restricted range of Fa values
656 characterizes the redox conditions at which metamorphism occurred. These conditions were more

657 reducing than those for the CV and CR meteorites, since mean Fa values of olivine in metamorphosed
658 samples from these groups are much higher. For example, olivine in the CV4 chondrite NWA 8418
659 (Mallozzi et al., 2018), originally classified as C3 (MBDB), shows a mean Fa value of ~40 mol%, with a
660 pronounced peak at ~38 mol%, far away from the Fa values in CL samples. The CR6 chondrites NWA
661 6921, NWA 7317, and NWA 11561 show mean Fa values between 29 and 38 mol% (MBDB), which is
662 also much higher than in CL chondrites. Due to these differences it is obvious that CL chondrites do
663 not represent thermally altered CV and CR chondrites.

664

665 5.1.4 Fe-Ni metal abundance

666 Another distinctive feature of CL compared to CV chondrites is the high amount of Fe-Ni metal,
667 which influences their magnetic properties. The magnetic susceptibility of LoV 051, the least
668 weathered sample, is $\log\chi = 5.24$ (where χ is in $10^{-9} \text{ m}^3 \cdot \text{kg}^{-1}$), which is similar to the mean value for CR
669 chondrites of $\log\chi = 5.04 \pm 0.12$ (Table 3; Rochette et al., 2008). The value for the saturation
670 magnetization M_S ($32.3 \text{ Am}^2/\text{kg}$) translates into a kamacite content of 14.4 wt.% for LoV 051. The
671 hysteresis properties of the investigated samples are similar to those of Renazzo CR chondrite. They
672 are markedly different from those of CV chondrites (Weisberg et al., 1997), including CV_{red} that show
673 the highest Fe-Ni metal abundances. Indeed, CV_{red} meteorites contain much less metal than LoV 051,
674 i.e. $2.73 \pm 1.12 \text{ vol}\%$ (average \pm s.d., $n=9$; Bonal et al., 2020), translating into $6.8 \pm 2.8 \text{ wt}\%$.

675

676 5.1.5 CAI abundances

677 The CAI abundances appear to be another characteristic property of the CL chondrites, although
678 our data base is limited. The modal abundance of CAIs is highly variable (from 0.1 vol% for Coolidge
679 to 8 vol% for Loongana; Table 2), probably due to the small section sizes ($52 - 361 \text{ mm}^2$; Table 1). It
680 was shown by Hezel et al. (2008) that section sizes $<1000 \text{ mm}^2$ do not give representative results, as
681 CAI abundances follow a Poisson distribution in thin sections. Taking all measurements together (655
682 mm^2), the average CAI abundance is 1.4 vol%. Hence, our best guess for the CAI concentration in
683 these samples is ~1.4 vol%, which is much higher than in CR chondrites (0.12 vol%) and distinctly
684 lower than in CV chondrites (~3 vol% or ~4 vol%; Hezel et al., 2008; Ebel et al, 2016). Our estimate is
685 comparable to that given in Kallemeyn and Rubin (1995) for Coolidge and Loongana (1-2 vol%).

686

687 5.1.6 Inter-chondrule matrix

688 Complementary to the high chondrule concentration, the low amount of inter-chondrule matrix (17-
689 21%; Table 2) is another important distinctive feature of CL chondrites. The mean modal abundances
690 of matrix in CV and CR chondrites are much higher, i.e., 52 vol% and 40 vol% in CV_{ox} and CV_{red},
691 respectively, (Gattacceca et al., 2020) and 35 vol% in CR chondrites (Schrader et al., 2011). Our value
692 of 18% for Coolidge is nearly identical to the value (17.6%) given by McSween (1977a). The value for
693 matrix in Coolidge as obtained by Kallemeyn and Rubin (1995) is higher (~30%), but may reflect
694 sample inhomogeneity. Their value for matrix abundance in Loongana is ~20%, identical to the value
695 found in the present study (Table 2).

696 It was found by Noguchi (1994) that Coolidge matrix is depleted in Na, compared to the reduced
697 CV chondrite Efremovka. This can be confirmed by our measurements, since we found a Na₂O

698 concentration of 0.25 wt.% in Coolidge matrix, which is only half the concentration found in Vigarano
699 Matrix (0.54 wt.%; McSween and Richardson, 1977; [Table 8](#)). However, the Na₂O concentration in CL
700 matrix varies considerably between 0.09 wt.% (NWA 13400) and 0.53 wt.% (NWA 033), with a mean
701 value of 0.30 wt.% ([Table 8](#)). The mean concentration of Al₂O₃ in CL chondrite matrix (1.84 wt.%) is
702 considerably lower than in the matrices of the various CV chondrite subgroups, as well as in CR and
703 CK chondrites (2.04-7.63 wt.%; [Table 8](#)). Another striking difference is the enrichment of Cr₂O₃ (mean
704 value 0.71 wt.%) in the CL chondrite matrix, compared to 0.35-0.44 wt.% in CV, CK, and CR
705 chondrites ([Table 8](#)). This characteristic was already described by McSween and Richardson (1977)
706 for the Coolidge chondrite. The clearest difference to matrix compositions of CR, CK, and the different
707 CV chondrite subgroups are the extraordinarily high MgO concentrations in the matrices of the
708 investigated CL samples (mean 28.3 wt.%), compared to mean values of 18.2-21.7 wt.% in the other
709 groups ([Table 8](#)). Furthermore, S is considerably depleted in the CL matrix (mean value 0.14 wt.%),
710 compared to CR chondrites and the CV_{red} and CV_{oxA} groups. Only CK chondrites show a lower mean
711 concentration (0.09 wt.%). However, CL3.9/CL4 and CK4 chondrites were affected by thermal
712 metamorphism on their parent asteroids, by which the fine-grained matrix may have undergone
713 considerable chemical modifications.

714

715 *5.1.7 Bulk chemical compositions*

716 The most characteristic chemical difference between CL chondrites and all other carbonaceous
717 chondrite groups (besides CB and CH) is their strong depletion of volatile lithophile and chalkophile
718 elements. The differences to the CV chondrite Allende can be seen in [Tables 9-10](#) and [Figs. 9-10](#).
719 This distinctive feature was previously noticed for Coolidge and Loongana (e.g. Kallemeyn and
720 Wasson, 1982; Kallemeyn and Rubin, 1995; Weckwerth, 2014). The CL chondrites are well resolved
721 from other carbonaceous chondrite groups on, for example Al₂O₃ vs. MnO ([Fig. 8a](#)), Al₂O₃ vs. Zn ([Fig.](#)
722 [8b](#)), and Zr vs. Rb ([Fig. 8c](#)) plots, since volatile elements like Mn, Zn, and Rb are moderately to
723 strongly depleted.

724 In [Fig. 9a](#) the CI-normalized concentrations (Lodders et al., 2009) of all measured lithophile
725 elements in the CL samples and the Allende reference sample are shown (see [Table 10](#)), together
726 with Allende literature data (dotted line). Elements in [Figs. 9 and 10](#) are arranged in the order of
727 increasing volatility (Wood et al., 2019). While elements from Zr (most refractory) to ~Eu in the CL
728 chondrites and Allende exhibit similar CI-normalized abundances, elements from V to Cs are
729 increasingly depleted. This trend steepens for elements more volatile than Cr (Mn, Na, K, Rb, and Cs),
730 with much stronger depletions in the CLs compared to Allende. This can also be seen in the mean CL
731 values in [Fig. 9b](#), when compared to mean values for the other carbonaceous chondrite groups (CM,
732 CO, CV, CR, CK4). The CL chondrites are characterized by strong enrichments of refractory and the
733 strongest depletions for volatile elements among all carbonaceous chondrite groups.

734 [Figure 10](#) shows the CI-normalized concentrations of siderophile and chalkophile elements in CL
735 chondrites. In [Fig. 10a](#) the values for individual CL chondrites are given, again in comparison to
736 Allende values (measurements and literature data). In [Fig. 10b](#) the mean CL values are given,
737 compared to the mean values of the other main carbonaceous chondrite groups. For the siderophile
738 elements Mo, Ni, Co, Fe, and P all samples show a similar pattern, which is also similar to that of the

739 Allende chondrite (Fig. 10a). The mean CL values (Fig. 10b) are in the range of those in the other
740 groups, with the highest concentration of Mo, the most refractory element in this plot. The chalcophile
741 element concentrations in the CL chondrites show some scatter, but are consistently lower than in
742 Allende (Fig. 10a). The mean CL values for chalcophile elements are plotted in Fig. 10b, compared to
743 mean values for the other carbonaceous chondrite groups. The CL mean values indicate the strongest
744 depletions of these elements compared to all other groups, which is in line with the strong depletions
745 of volatile lithophile elements (Fig. 9). Recently, Braukmüller et al. (2018) have shown that the major
746 groups of carbonaceous chondrites show about the same depletions for the most volatile elements.
747 Specifically, these authors observed that volatile elements with 50% condensation temperatures below
748 800 K (from Zn to Tl in Fig. 10) are depleted to about the same extent and they, therefore, termed
749 them “plateau volatile elements”. The CL chondrites investigated in this study seem to deviate from a
750 plateau-like pattern, since the Zn, Pb, and Tl concentrations appear low compared to the Se and Te
751 concentrations (Fig. 10b). However, Braukmüller et al. (2018) also showed that in the ungrouped
752 carbonaceous chondrite EET 96026 the relative concentrations of the plateau volatile elements were
753 strongly modified during thermal metamorphism. As such, the deviations for the CL chondrites
754 observed in this study most likely also reflect element fractionations during thermal metamorphism.
755 This issue will be further discussed below (section 5.2).

756

757 5.1.8 Bulk isotopic compositions

758 Figure 11 shows that the O isotopic compositions of CL chondrites (Table 11) do not define a tight
759 cluster, but exhibit a range of isotopic compositions along the CCAM line ($\Delta^{17}\text{O}$ -3.96 to -5.47‰). This
760 is also typical of the CV and CK groups and may be indicative of some form of genetic relationship
761 between these groups. Two samples (Coolidge, LoV 051) fall outside the compositional fields of CV
762 and CK chondrites and have considerably lower $^{17}\text{O}/^{16}\text{O}$ and $^{18}\text{O}/^{16}\text{O}$ ratios. However, Gattacceca et
763 al. (2020) presented O isotope data of two Antarctic CV_{red} chondrites, which overlap with our values
764 for Coolidge. On the other hand, the O isotopic compositions of CL chondrites are clearly distinct from
765 CR chondrites, ruling out any genetic link between these two chondrite groups.

766 The investigated CL samples have a mean $\epsilon^{54}\text{Cr}$ value of 0.71 ± 0.06 (Table 12) and are therefore
767 characterized by a slightly lower $\epsilon^{54}\text{Cr}$ than CV chondrites (mean $\epsilon^{54}\text{Cr} = 0.87 \pm 0.07$; Burkhardt et
768 al., 2019) and can clearly be distinguished from the mean $\epsilon^{54}\text{Cr}$ values of CM and CR chondrites (Fig.
769 12; Trinquier et al., 2007; Qin et al., 2010). The only known carbonaceous chondrite group with similar
770 $\epsilon^{54}\text{Cr}$ are the CO chondrites. By contrast, all CL samples exhibit significantly lower $\epsilon^{50}\text{Ti}$ values than
771 typically observed for CV, CO, and CK groups (e.g. Trinquier et al., 2009; Zhang et al., 2012;
772 Burkhardt et al., 2019), and their weighted mean $\epsilon^{50}\text{Ti}$ of 2.60 ± 0.05 (Table 12) is also significantly
773 lower than the $\epsilon^{50}\text{Ti}$ of 3.21 ± 0.11 measured for bulk Allende (CV3) in the present study. The Ti
774 isotopic composition of CL chondrites is more similar to that of CM and CR chondrites (Fig. 12b). On a
775 plot of $\epsilon^{50}\text{Ti}$ vs $\epsilon^{54}\text{Cr}$ the CL chondrites define a distinct cluster with a unique position. Thus, this plot is
776 particularly useful as a means of demonstrating that the CL chondrites are isotopically distinct from the
777 other carbonaceous chondrite groups.

778 The Ti isotopic variability among carbonaceous chondrites may be primarily related to the varying
779 CAI abundances of the different chondrite groups (Burkhardt et al., 2019), as CAIs are highly enriched

780 in Ti and are characterized by large $\epsilon^{50}\text{Ti}$ excesses (e.g., $\epsilon^{50}\text{Ti} \approx 9$; Render et al., 2019). For instance,
781 CAI-free CI chondrites display the lowest $\epsilon^{50}\text{Ti}$ excesses among the carbonaceous chondrites,
782 whereas CAI-rich CV, CO, and CK chondrites exhibit large $\epsilon^{50}\text{Ti}$ excesses (e.g. Trinquier et al., 2009).
783 As such, the less-pronounced $\epsilon^{50}\text{Ti}$ excesses of the CL chondrite samples relative to CV, CO, and CK
784 chondrites suggest that CL chondrites are characterized by significantly lower CAI abundances
785 compared to the other groups of carbonaceous chondrites. This is in line with petrographic
786 observations, since CL chondrites contain about 1.4 vol% of CAIs (see sections 4.7.2 and 5.1.5), in
787 contrast to ~3 vol% in CV chondrites (Hezel et al., 2008). Contrary to Ti, CAIs are strongly depleted in
788 Cr relative to the major components of chondrites (e.g., chondrules and matrix), and so varying CAI
789 abundances have a negligible effect on the Cr isotopic composition of bulk chondrites. Consistent with
790 this, the $\epsilon^{54}\text{Cr}$ values of CL chondrites are comparable to those of the CAI-rich CV, CO, and CK
791 chondrites (Fig. 12). Of note, given the large amount of sample material provided for analysis, it is
792 likely that the less-pronounced $\epsilon^{50}\text{Ti}$ excesses of the CL chondrite samples relative to CV, CO, and CK
793 chondrites are genuine features, and are not related to sampling bias (e.g., lower CAI abundances in
794 the selected sample aliquot).

795

796 **5.2 Volatile depletions: nebular fractionation or thermal metamorphism on the parent body?**

797

798 The low concentrations of volatile elements in Coolidge, Loongana and the three other CL samples
799 is probably a reflection, to some extent, of their relatively low modal abundance of inter-chondrule
800 matrix (17-21%; Table 2). This component is usually the carrier of volatile elements and its abundance
801 in CL chondrites is only about half as high as in the CV and CR chondrites (40% and 30-50%; Krot et
802 al., 2014). On the other hand, the samples were heated on their parent asteroid, which might have
803 caused volatile loss. This effect was investigated for Allende (CV_{oxA}; Wulf et al. (1995) and for
804 Murchison (CM2; Braukmüller et al. (2018) with heating experiments under oxidizing and reducing
805 conditions. Since the five CL meteorites are characterized by high original amounts of Fe-Ni metal, the
806 thermal metamorphism most likely occurred under reducing conditions. The depletions of the volatile
807 lithophile elements Mn, Na, K, Rb, and Cs is one of the most distinctive features of CL chondrites
808 (Figs. 8a, 9). However, Braukmüller et al (2018) did not observe considerable depletions of these
809 elements during their heating experiments (Mn was not considered). The behavior of Mn was
810 investigated by Wulf et al (1995) who found that Mn does not show any depletions, even not in the
811 experiments performed at 1300°C, neither under oxidizing nor reducing conditions. Considerable
812 depletions of chalcophile elements like Zn, Te, Pb, and Tl were found by Wulf et al. (1995) and
813 Braukmüller et al. (2018) under reducing conditions. However, the experimentally produced depletion
814 of Pb is higher than for Zn (Braukmüller et al., 2018), whereas these two elements are depleted in CL
815 chondrites to about the same extent (Fig. 10b). From these observations we conclude that the
816 consistently low bulk concentrations of the volatile lithophile elements (Mn, Na, K, Rb, and Cs) and the
817 chalcophile elements (Zn, Se, Te, Pb and Tl) in CL chondrites are a primary feature and do not result
818 from thermal metamorphism on the parent body. However, it is possible that the latter process affected
819 the chalcophile element concentrations in the CL samples to some extent. In particular, the relative
820 abundances of the plateau volatile elements appear to have been modified by this process, because

821 the ratios of these elements vary considerably among individual CL samples (Fig. 10a), possibly
822 indicating local redistribution on the parent body.

823

824 **5.3 Proposal for the new Loongana (CL) group of carbonaceous chondrites**

825

826 Based on their common characteristics we conclude that the five investigated meteorites can be
827 combined together to form a new group of carbonaceous chondrites. The foundation for this was given
828 by Kallemeyn and Rubin (1995), who defined the Coolidge-Loongana grouplet.

829

830 *5.3.1 Proposed naming as the CL group of carbonaceous chondrites*

831 Among the investigated samples only Coolidge was given an individual meteorite name; the others
832 are named by serial numbers (Table 1). Hence, the first alphabetic character of Coolidge would be the
833 best candidate to name this group, leading to the CC group of carbonaceous chondrites, which is
834 precluded by the already existing CC meteorite class (CC for carbonaceous chondrites). Since
835 Loongana 001 was the first meteorite for which a close relation to Coolidge was described (Kallemeyn
836 and Rubin, 1995), we propose to use its first alphabetic character for naming this new group as the CL
837 group.

838

839 *5.3.2 Other meteorites proposed to belong to the Coolidge-Loongana grouplet*

840 There are some other ungrouped carbonaceous chondrites, which may belong to the Coolidge-
841 Loongana grouplet. However, as will be argued below, none of these samples share the characteristic
842 properties of the five CL chondrites of this study. Nevertheless, future determination of Ti and Cr
843 isotopic compositions of these meteorites will probably help to clarify their relationship to the CL
844 chondrites and other groups of carbonaceous chondrites.

845

846 *5.3.2.1 NWA 779*

847 Weckwerth et al. (2001) proposed that NWA 779 belongs to the Coolidge-Loongana grouplet.
848 However, the determined mean Fa concentration in olivine is 21 mol%, largely different from the Fa
849 values of Loongana (12.5 mol%), Coolidge (14.5 mol%) and the other samples described by us (12.8-
850 14.7 mol%; Table 4). Several volatile element concentrations are considerably higher in NWA 779.
851 These are, for example K₂O (0.08 wt.% in NWA 779 compared to 0.01-0.02 wt.% in the CLs; Table 9),
852 MnO (0.20 wt.% compared to 0.14-0.16 wt.%; Table 9), and Zn (110 ppm compared to 33-57 ppm;
853 Table 10). A further obvious difference is the low concentration of Ni and Co in NWA 779 (6000 and
854 300 ppm, respectively), compared to 12800-13900 ppm and 560-600 ppm, respectively, in the five
855 investigated CL meteorites (Table 9). This is difficult to explain by terrestrial weathering, since most of
856 the CL samples are also strongly weathered. Obviously, NWA 779 contains (as a primary feature)
857 much lower amounts of Fe-Ni metal than the CL meteorites. For these reasons, NWA 779 does not
858 belong to the proposed CL group, but appears to be correctly classified as CV3 (of high petrologic
859 type) in the MBDB.

860

861 *5.3.2.2 Hammada al Hamra (HaH) 073*

862 Weckwerth and Weber (1998) and Weckwerth (2014) conclude that Hammada al Hamra (HaH)
863 073, currently classified as C4 (MBDB), belongs to the Coolidge-Loongana grouplet. The O isotopic
864 composition of this sample plots within the range of CV-CK chondrites on the CCAM line in $\delta^{18}\text{O}$ - $\delta^{17}\text{O}$
865 space (MBDB). Its mean Fa content in olivine is 17.9 mol%, i.e. outside the range of the five
866 investigated CL samples (12.5-14.7 mol%) and it contains considerably more (~33 vol%) fine-grained
867 matrix (Weckwerth and Weber, 1998) than the here studies samples (17-21 vol%; Table 2). The mean
868 apparent chondrule size of HaH 073 is 580 μm (Weckwerth and Weber, 1998), also outside the range
869 of the measured CL values (404-477 μm ; Table 7). The concentrations of Ni and Co in HaH 073
870 (12600 and 575 ppm, respectively; Choe et al., 2010) are slightly lower than those in the CL samples
871 (12800-13900 ppm and 560-600 ppm, respectively; Table 9), indicating a slightly lower abundance of
872 Fe-Ni metal. The concentrations of many volatile elements in HaH 073 are considerably higher than in
873 CL chondrites. The Na_2O concentrations in the latter are 0.18-0.32 wt.% (Table 9), compared to 0.51
874 (Weckwerth and Weber, 1998) and 0.50 (Choe et al., 2010), respectively, in HaH 073. The same is
875 true for K, which shows low concentrations of 0.01-0.02 wt.% in CL chondrites (Table 9) and high
876 concentrations between 0.034 (Choe et al., 2010) and 0.040 wt.% (Weckwerth and Weber, 1998) in
877 HaH 073. The MnO concentration in HaH 073 (0.17 wt.%; Weckwerth and Weber, 1998; Choe et al.,
878 2010) is somewhat higher than in the CL samples (0.14-0.16 wt.%), and the Zn concentration is
879 distinctly higher, namely 63-66 ppm (Weckwerth and Weber, 1998; Choe et al., 2010), compared to
880 33-57 ppm in our samples. However, Weckwerth (2014) revised several HaH 073 values from an
881 earlier publication (Weckwerth and Weber, 1998) and some of the new results are closer to the range
882 of CL values, e.g., MnO (0.13 wt.%) and Zn (20 ppm). However, the new data for Na_2O (0.43 wt.%)
883 and K_2O (0.037 wt.%) are still much higher than those in the CL chondrites. Taking the above
884 differences together, it appears that HaH 073 may be related to, but is not a full member of the CL
885 chondrite group.

886

887 5.3.2.3 Sahara 00182

888 Weckwerth (2014) argued that Sahara 00182 (C3-ung; MBDB) belongs to the Coolidge-Loongana
889 grouplet. This meteorite with a mean Fa value of 7.8 mol% (Smith et al., 2004) is probably paired with
890 Sahara 00177 (C3/4-ung; MBDB), which shows a mean Fa value of 7.6 mol%. These Fa values are
891 far outside the range for CL chondrites (12.5-14.7 mol%). Due to the absence of phyllosilicates,
892 Weisberg (2001) classified Sahara 00182 as the first CR3 chondrite. However, its oxygen isotopic
893 composition plots on the CCAM line in $\delta^{18}\text{O}$ - $\delta^{17}\text{O}$ space (MBDB), which excludes a relationship to CR
894 chondrites. A mean apparent chondrule size of 1010 μm was determined by Smith et al (2004), a
895 much higher value compared to the CL samples (404-474 μm ; Table 7). The modal abundance of
896 inter-chondrule matrix is ~28 vol% (Smith et al., 2004), a value which is outside the observed range in
897 CL chondrites (17-21 vol%; Table 2). The concentration of Ni and Co in Sahara 00182 (14900 and 691
898 ppm, respectively; Choe et al., 2010) are higher than CL values (12800-13900 ppm and 560-600 ppm,
899 respectively; Table 9), indicating a higher abundance of Fe-Ni metal. Furthermore, Na_2O and K_2O
900 concentrations in Sahara 00182 are higher than in the CL chondrites, namely 0.29-0.36 and 0.03
901 wt.%, respectively (Choe et al., 2010; Weckwerth, 2014), compared to 0.18-0.27 wt.% and 0.01-0.02
902 wt.% (Table 9). Due to these differences it is improbable that Sahara 00182 is closely related to the CL

903 chondrites. The strongest argument against such a relationship is provided by the distinctly different
904 chemical composition of inter-chondrule matrix. The SiO₂ and MgO concentrations in the matrix of
905 Sahara 00182 are 24.2 and 21.7 wt.%, respectively, compared to 30.3 and 28.3 wt.% in the CL
906 chondrites (Table 8). These values from Smith et al. (2004) have been recalculated to totals of 95
907 wt.% for comparison. There are even more extreme differences in the matrix concentrations of CaO
908 and S. While the matrix in CL chondrites is characterized by very low concentrations of CaO and S
909 (0.97-1.61 wt.% and 0.04-0.35 wt.%, respectively; Table 8), matrix in Sahara 00182 contains 5.75
910 wt.% CaO and 2.50 wt.% S (Smith et al., 2004).

911

912 *5.3.3 Anticipated characteristics of unmetamorphosed, yet to be detected samples*

913 Since all investigated CL meteorites are affected by thermal metamorphism (petrologic types 3.9 to
914 4; Table 2) the question remains how unmetamorphosed samples might look like. It cannot be ruled
915 out that such samples are hidden among the tangled mass of CV_{red} and CR chondrites from Northwest
916 Africa (NWA) and other dense collection areas. On a first glance, those samples would appear
917 unusual due to their very high chondrule abundances and the correspondingly low amounts of fine-
918 grained inter-chondrule matrix (Table 2). Depending on the weathering grade, they would more or less
919 stand out against CV_{red} chondrites by their high metal content and high magnetic susceptibility (Table
920 3). The O isotopic compositions would plot on the CCAM line, within the range of CV-CK chondrites or
921 to the direction of lighter isotopes (Fig. 12). In the end, unmetamorphosed CL chondrites would be
922 definitely uncovered by their characteristic depletions of volatile lithophile and chalkophile elements
923 (Figs. 9, 10), and their Ti and Cr isotopic compositions (Fig. 12b).

924

925 **5.4 Possible genetic relationships between CL chondrites and CV and CK chondrites**

926

927 The recognition of a further distinct carbonaceous chondrite group raises questions about how the
928 characteristics of each of these groups was initially established. Oxygen and Cr isotopic data as well
929 as chondrule size-frequency distributions suggest a relationship between the CL chondrites and CV
930 and CK chondrites. Perhaps their parent bodies formed in a similar nebular region (heliocentric
931 distance) distinct from those of the other carbonaceous chondrite groups. Compared to CV and CK
932 asteroids, the CL asteroid(s) obviously formed from a distinct mix of components, with higher amounts
933 of chondrules and lower amounts of CAIs and matrix. The low matrix content may indicate a
934 correspondingly low amount of co-accreted water ice which led to more reducing conditions during
935 thermal metamorphism.

936 However, most CV chondrites are of low petrologic type (3.1-3.6; e.g. Bonal et al., 2006), which is
937 in strong contrast to CK and CL chondrites. Most CK chondrites are of petrologic type 4 to 6 and all yet
938 identified members of the CL group are of petrologic types 3.9 to 4 (Table 2). One explanation for
939 these differences is a possible bias of material delivery to Earth by secondary parent bodies, which are
940 in a suitable resonance position just by chance. Greenwood et al. (2020) discuss the relationship
941 between primary and secondary parent bodies, where the latter derived from the former through
942 impact break-up. By this process, secondary bodies form, which do not fully represent the material of
943 the primary body. Even if all primary bodies would have had a similar, for example, onion shell

944 structure of petrologic types (type 6 in the interior, types 5-3 in the outer layers), secondary fragments
945 would mostly consist of material with a restricted range of petrologic types. These types would be
946 overrepresented in our collections, if such secondary parent bodies are the main source of a given
947 meteorite group (e.g., CL chondrites) due to their favorite resonance position.

948

949

6. SUMMARY AND CONCLUSIONS

950

951 The five ungrouped carbonaceous chondrites Coolidge, Loongana 001, LoV 051, NWA 033, and
952 NWA 13400 can be grouped together to establish the Loongana (CL) group of carbonaceous
953 chondrites. Based on the presented data we conclude that CL chondrites are characterized by:

954

955 1. Fe-Ni metal abundances considerably higher than for CV chondrites, but similar to CR
956 chondrites

957 2. Chondrule size-frequency distributions similar to CV chondrites, but dissimilar to CR chondrites

958 3. Mean CAI abundances of ~1.4 vol%, i.e. lower than in CV, but much higher than in CR
959 chondrites

960 4. Very low amounts of inter-chondrule matrix (17-21 vol%), the lowest among the main
961 carbonaceous chondrite groups (CI, CY, CM, CO, CV, CR, CK)

962 5. Nearly equilibrated olivine with mean fayalite (Fa) values between 12.5 mol% (Loongana) and
963 14.7 mol% (NWA 13400) as a metamorphic effect

964 6. Lower Al₂O₃ and higher MgO and Cr₂O₃ concentrations in inter-chondrule matrix compared to
965 matrix in CV, CK, and CR chondrites, as a possible metamorphic effect

966 7. Considerable bulk depletion of the volatile lithophile elements Mn, Na, K, Rb, and Cs, and the
967 chalcophile elements Zn, Se, Te, Pb, and Tl, compared to all other main carbonaceous
968 chondrite groups

969 8. Bulk O isotope compositions plotting along the CCAM line ($\Delta^{17}\text{O}$ -3.96 to -5.47‰), partly
970 overlapping with the CV and CK chondrite field but including samples that are ¹⁶O-enriched

971 9. Unique positions in the $\epsilon^{54}\text{Cr}$ - $\epsilon^{50}\text{Ti}$ isotope plot, with $\epsilon^{54}\text{Cr}$ values similar to CV and $\epsilon^{50}\text{Ti}$ values
972 similar to CR chondrites.

973

974 Loongana-type (CL) chondrites show many similarities to CV and CK chondrites and may have
975 accreted from the same nebular reservoir. Although the average magnetic susceptibility of CL
976 chondrites is similar to CR chondrites, these groups are not related. This is mainly indicated by their
977 different isotopic compositions of O (Figs. 12, 13a) and Ti (Fig. 13b), but also by their different size-
978 frequency distributions of apparent chondrule sizes (Table 7, Fig. 5).

979 The interesting question remains, if unidentified or misidentified CL members of lower petrologic
980 types are hidden in our collections, possibly among the large number of CV_{red} and CR chondrites from
981 hot and cold deserts. Such samples would be important to investigate the pristine state of these
982 meteorites and their components.

983

984

985
986
987
988
989
990
991
992
993
994
995
996
997
998
999
1000
1001
1002
1003
1004
1005
1006
1007
1008
1009
1010
1011
1012
1013
1014
1015
1016
1017
1018
1019
1020
1021
1022
1023
1024
1025

ACKNOWLEDGEMENTS

We thank Dr. Jutta Zipfel (Senckenberg Forschungsinstitut und Naturmuseum, Frankfurt, Germany) and Mirko Graul (Bernau, Germany) for providing samples of Loongana 001 and NWA 13400, respectively. This work was supported by the Deutsche Forschungsgemeinschaft (DFG, German Research Foundation), grant number ME 1115/10-1 and Project-ID 263649064 – TRR 170. This is TRR 170 pub. no. XX.

REFERENCES

Alexander C. M. O'D., Greenwood R. C., Bowden R., Gibson J. M., Howard K. T. and Franchi I. A. (2018) A multi-technique search for the most primitive CO chondrites. *Geochim. Cosmochim. Acta* **221**, 406-420.

Barosch J., Hezel D. C., Ebel D. S. and Friend P. (2019) Mineralogically zoned chondrules in ordinary chondrites as evidence for chondrule open system behavior. *Geochim. Cosmochim. Acta* **249**, 1–16.

Barosch J., Hezel D. C., Sawatzki L., Halbauer L. and Marrocchi Y. (2020) Sectioning effects of porphyritic chondrules: implications for the PP/POP/PO classification and correcting modal abundances of mineralogically zoned chondrules. *Meteorit. Planet. Sci.*, doi: <https://doi.org/10.1111/maps.13476>

Barrat J.-A., Zanda B., Moynier F., Bollinger C., Liorzou C. and Bayon G. (2012) Geochemistry of CI chondrites: major and trace elements, and Cu and Zn Isotopes. *Geochim. Cosmochim. Acta* **83**, 79–92.

Bence A. E. and Albee A. L. (1968) Empirical correction factors for the electron micro-analysis of silicates and oxides. *J. Geol.* **76**, 382–403.

Bischoff A., Palme H., Ash R. D., Clayton R. N., Schutz L., Herperts U., Stöffler D., Grady M. M., Pillinger C. T., Spettel B., Weber H., Grund T., Endreß M. and Weber D. (1993) Paired Reanazzo-type (CR) carbonaceous chondrites from the Sahara. *Geochim. Cosmochim. Acta* **57**, 1587-1603.

Bonal L., Quirico E., Bourrot-Denise M. and Montagnac G. (2006). Determination of the petrologic type of CV3 chondrites by Raman spectroscopy of included organic matter. *Geochim. Cosmochim. Acta* **70**, 1849-1863.

Bonal L., Gattacceca J., Garenne A., Eschrig J., Rochette P. and Krämer Ruggiu L. (2020) Water and heat: new constraints on the evolution of the CV chondrite parent body. *Geochim. Cosmochim. Acta*, doi.org/10.1016/j.gca.2020.03.009

Braukmüller N., Wombacher F., Hezel D. C., Escube R. and Münker C. (2018) The chemical composition of carbonaceous chondrites: Implications for volatile element depletion, complementarity and alteration. *Geochim. Cosmochim. Acta* **239**, 17-48.

Burkhardt C., Hi. R. C., Kleine T. and Bourdon B. (2014) Evidence for Mo isotope fractionation in the solar nebula and during planetary differentiation. *Earth Planet. Sci. Lett.* **391**, 201-211.

Burkhardt C., Dauphas N., Tang H., Fischer-Gödde M., Qin L., Chen J. H., Rout S. R., Pack A., Heck P. R. and Papanastassiou D. A. (2017) In search of the Earth-forming reservoir: Mineralogical,

1026 chemical, and isotopic characterizations of the ungrouped achondrite NWA 5363/NWA 5400 and
 1027 selected chondrites. *Meteorit. Planet. Sci.* **52**, 807-826.

1028 Burkhardt C., Dauphas N., Hans U., Bourdon B. and Kleine T. (2019) Elemental and isotopic variability
 1029 in solar system materials by mixing and processing of primordial disk reservoirs. *Geochim.*
 1030 *Cosmochim. Acta* **261**, 145–170.

1031 Choe W. H., Huber H., Rubin A. E., Kallemeyn G. W. and Wasson J. T. (2010) Compositions and
 1032 taxonomy of 15 unusual carbonaceous chondrites. *Meteorit. Planet. Sci.* **45**, 531-554.

1033 Clayton R. N. and Mayeda T. K. (1999). Oxygen isotope studies of carbonaceous chondrites.
 1034 *Geochim. Cosmochim. Acta* **63**, 2089-2104.

1035 Dauphas N. and Schauble E. A. (2016) Mass Fractionation Laws, Mass-Independent Effects, and
 1036 Isotopic Anomalies. *Annu. Rev. Earth Planet. Sci.* **44**, 709–783.

1037 Ebel D. S., Brunner C., Konrad K., Leftwich K., Erb, I., Lu M., Rodriguez H., Crapster-Pregont E. J.,
 1038 Friedrich J. M., and Weisberg M. K. (2016) Abundance, major element composition and size of
 1039 components and matrix in CV, CO and Acfer 094 chondrites. *Geochim. Cosmochim. Acta* **172**,
 1040 322-356.

1041 Eisenhour D. D. (1996) Determining chondrule size distributions from thin-section measurements.
 1042 *Meteorit. Planet. Sci.* **31**:243-248.

1043 Feldstein S. N., Jones R. H. and Papike J. J. (2001) Disequilibrium partial melting experiments on the
 1044 Leedey L6 chondrite: Textural controls on melting processes. *Meteorit. Planet. Sci.* **36**,1421–1441.

1045 Friend P., Hezel D. C. and Mucerschi D. (2016) The conditions of chondrule formation, Part II: Open
 1046 system. *Geochim. Cosmochim. Acta* **173**, 198–209.

1047 Gattacceca J., Suavet C., Rochette P., Weiss B.P., Winkhofer M., Uehara M. and Friedrich J. (2014)
 1048 Metal phases in ordinary chondrites: magnetic hysteresis properties and implications for thermal
 1049 history. *Meteorit. Planet. Sci.* **49**, 652-676.

1050 Gattacceca J., Bonal L., Sonzogni C. and Longerey J. (2020) CV chondrites: more than one parent
 1051 body. *Earth Planet. Sci. Lett.* **547**, doi.org/10.1016/j.epsl.2020116467.

1052 Greenwood R. V., Franchi I. A., Kearsley A. T. and Alard O. (2010) The relationship between CK and
 1053 CV chondrites. *Geochim. Cosmochim. Acta* **74**, 1684-1705.

1054 Greenwood R. C., Burbine T. H., Miller M. F. and Franchi I. A. (2017) Melting and differentiation of
 1055 early-formed asteroids: The perspective from high precision oxygen isotope studies: *Chemie der*
 1056 *Erde-Geochemistry* **77**, 1-43.

1057 Greenwood R.C., Burbine T. H. and Franchi I.A. (2020) Linking asteroids and meteorites to the
 1058 primordial planetesimal population *Geochim. Cosmochim. Acta* **277**, 377-406.
 1059 <https://doi.org/10.1016/j.gca.2020.02.004>.

1060 Griffin W. L., Powell W. J., Pearson N. J. and O'Reilly S.Y. (2008) GLITTER: data reduction software
 1061 for laser ablation ICP-MS, in Sylvester, P., ed., *Laser Ablation ICP-MS in the Earth Sciences:*
 1062 *Current Practices and Outstanding Issues*, Mineralogical Association of Canada. Short Course
 1063 Series **40**, 308-311.

1064 Guimon R. K., Symes S. J. K., Sears D. W. G. Sears and Benoit P (1995) Chemical and physical
 1065 studies of type 3 chondrites XII: The metamorphic history of CV chondrites and their components.
 1066 *Meteorit. Planet. Sci.* **30**, 704-714.

- 1067 Hezel D. C. (2010) A mathematica code to produce phase maps from two element maps. *Computers*
1068 & *Geosciences* **36**, 1097–1099.
- 1069 Hezel D. C. and Palme H. (2008) Constraints for chondrule formation from Ca-Al distribution in
1070 carbonaceous chondrites. *Earth Planet. Sci. Lett.* **265**, 716-725.
- 1071 Hezel D. C., Russell S. S., Ross A. J., and Kearsley A. T. (2008) Modal abundances of CAIs:
1072 Implications for bulk chondrite element abundances and fractionations. *Meteorit. Planet. Sci.* **43**,
1073 1879-1894.
- 1074 Hutchison R. (2004) *Meteorites - A petrologic, chemical and isotopic synthesis*. In Cambridge
1075 Planetary Science (ed. Bagenal F., Jewitt D., Murray C., Bell J., Lorenz R., Nimmo F., and Russell
1076 S. Cambridge, UK: Cambridge University Press. 506 p.
- 1077 Jarosewich E. (2006) Chemical analysis of meteorites at the Smithsonian Institution: An update.
1078 *Meteorit. Planet. Sci.* **41**, 1381-1382.
- 1079 Jarosewich E., Clarke R. S., Jr. and Barrows J. N. (1987) The Allende meteorite reference sample. In:
1080 *The Allende meteorite reference sample* (eds. E. Jarosewich, R. S. Clark, and J. N. Barrows),
1081 Smiths. Inst. Press, Washington D.C., pp. 1-12.
- 1082 Jochum K. P., Nohl U., Herwig K., Lammel E., Stoll B. and Hofmann, A.W. (2005) GeoReM: A New
1083 Geochemical Database for Reference Materials and Isotopic Standards. *Geostandards and*
1084 *Geoanalytical Research* **29-3**, 333-338.
- 1085 Jones R. H., Grossman J. N. and Rubin A. E. (2005). Chemical, mineralogical and isotopic properties
1086 of chondrules: Clues to their origin. In *Chondrites and the Protoplanetary Disk* (eds. A.N. Krot,
1087 E.R.D. Scott, and B. Reipurth). Astronomical Society of the Pacific Conference Series **341**, 251-
1088 285.
- 1089 Kallemeyn (1987) Compositional comparisons of metamorphosed carbonaceous chondrites. Mem.
1090 Natl. Inst. Polar Res., Spec. Issue, **46**, 151-161.
- 1091 Kallemeyn G. W. and Rubin A. (1995) Coolidge and Loongana 001: A new carbonaceous chondrite
1092 grouplet. *Meteoritics* **30**, 20-27.
- 1093 Kallemeyn G. W. and Wasson J. T. (1981) The compositional classification of chondrites: I. The
1094 carbonaceous chondrite groups. *Geochim. Cosmochim. Acta* **45**, 1217-1230.
- 1095 Kallemeyn G. W. and Wasson J. T. (1982) The compositional classification of chondrites: III.
1096 Ungrouped carbonaceous chondrites. *Geochim. Cosmochim. Acta* **46**, 2217-2228.
- 1097 Kallemeyn G. W., Rubin A. E. and Wasson J. T. (1991) The compositional classification of chondrites:
1098 V. The Karoonda (CK) group of carbonaceous chondrites. *Geochim. Cosmochim. Acta* **55**, 881-
1099 892.
- 1100 Kallemeyn G. W., Rubin A. E. and Wasson J. T. (1994) The compositional classification of chondrites:
1101 VI. The CR carbonaceous chondrite group. *Geochim. Cosmochim. Acta* **58**, 2873-2888.
- 1102 King A. J., Bates H. C., Krietsch D., Busemann H., Clay P. I., Schofield P. F. and Russell S. S. (2019)
1103 The Yamato-type (CY) carbonaceous chondrite group: Analogues for the surface of asteroid
1104 Ryugu? *Geochemistry* **79**, doi.org/10.1016/j.chemer.2019.08.003.
- 1105 Kleine T., Budde G., Burkhardt C., Kruijjer T. S., Worsham E. A., Morbidelli A. and Nimmo F. (2020)
1106 The Non-carbonaceous-Carbonaceous meteorite dichotomy. *Space Sci Rev.* **216**:55.

1107 Knab H.-J. (1981) The distributions of trace elements in carbonaceous chondrites. *Geochim.*
1108 *Cosmochim. Acta* **45**, 1563-1572.

1109 Krot, A. N., Keil, K., Scott, E. R. D., Goodrich, C. A. and Weisberg, M. K. (2014) Classification of
1110 meteorites and their genetic relationships. In: *Meteorites and Cosmochemical Processes*, Treatise
1111 on Geochemistry (Second Edition; ed. A. M. Davis). Elsevier, Vol. 1, pp.1-63.

1112 Krot A. N. (2019) Refractory inclusions in carbonaceous chondrites: Records of early solar system
1113 processes. *Meteorit. Planet. Sci.* **54**, 1647-1691.

1114 Lauretta D. S., Nagahara H. and Alexander C. M. O'D. (2006) Petrology and origin of ferromagnesian
1115 silicate chondrules. In: *Meteorites and the early solar system II*, edited by Lauretta D. S. and
1116 McSween H. Y. Tucson: The University of Arizona Press:431-459.

1117 Lodders K. (2003) Solar system abundances and condensation temperatures of the elements.
1118 *Astroph. J.* **591**, 1220-1247.

1119 Lodders K., Palme H. and Gail H. P. (2009) *Abundances of the elements in the solar system*. In:
1120 Landolt-Börnstein, New Series, vol. VI/4B (ed. J. E. Trümper). Springer, pp. 560-630.

1121 Mallozzi L., MacPherson G. J., Corrigan C. M., Irving A. J. and Pitt D. (2018) Northwest Africa 8418: A
1122 CV4 chondrite, with new insight into secondary processes on the CV parent body. In: *30th Lunar
1123 and Planetary Science Conference*, (abstract #2555).

1124 MBDB (Meteoritical Bulletin Database) <https://www.lpi.usra.edu/meteor/>.

1125 McCoy-West A. J., Millet M.-A. and Burton K. Y. (2017) The neodymium stable isotope composition of
1126 the silicate Earth and chondrites. *Earth Planet. Sci. Lett.* **480**, 121-132.

1127 McSween H. Y. Jr. (1977a) Petrographic variations among carbonaceous chondrites of the Vigarano
1128 type. *Geochim. Cosmochim. Acta* **41**, 1777-1790.

1129 McSween H. Y. Jr. (1977b) Chemical and petrographic constraints on the origin of chondrules and
1130 inclusions in carbonaceous chondrites. *Geochim. Cosmochim. Acta* **41**, 1843-1860.

1131 McSween H. Y. Jr. and Richardson S. M. (1977) The composition of carbonaceous chondrite matrix.
1132 *Geochim. Cosmochim. Acta* **41**, 1145-1161.

1133 Metzler K. (2012) Ultrarapid chondrite formation by hot chondrule accretion? Evidence from
1134 unequilibrated ordinary chondrites. *Meteorit. Planet. Sci.* **47**, 2193-2217.

1135 Matza S. D. and Lipschutz M. E. (1977) Volatile/mobile trace elements in Karoonda (C4) chondrite.
1136 *Geochim. Cosmochim. Acta* **41**, 1398-1401.

1137 Miller M. .F., Franchi I. A., Sexton A. S. and Pillinger C. T. (1999). High precision $\Delta^{17}\text{O}$ isotope
1138 measurements of oxygen from silicates and other oxides: Methods and applications. *Rapid Comm.
1139 Mass Spec.* **13**, 1211-1217.

1140 Millet M.-A. and Dauphas N. (2014) Ultra-precise titanium stable isotope measurements by double-
1141 spike high resolution MC-ICP-MS. *J. Analyt. Atom. Spectr.* **29**, 1444-1458.

1142 Mougel B., Moynier F. and Göpel C. (2018) Chromium isotopic homogeneity between the Moon, the
1143 Earth, and enstatite chondrites. *Earth Planet. Sci. Lett.* **481**, 1–8.

1144 Noguchi T. (1994) Petrology and mineralogy of the Coolidge meteorite (CV4). *Proc. NIPR Symp.
1145 Antarct. Meteorites* **7**, 42-72.

1146 Palme H. and Rammensee W. (1981) The cosmic abundance of molybdenum. *Earth Planet. Sci. Lett.*
1147 **55**, 356-362.

1148 Pourkhorsandi H., D’Orazio M., Rochette P., Valenzuela M., Gattacceca J., Mirnejad H., Sutter B.,
1149 Hutzler A., and Aboulahris M. (2017a) Modification of REE distribution of ordinary chondrites from
1150 Atacama (Chile) and Lut (Iran) hot deserts: Insights into the chemical weathering of meteorites.
1151 *Meteorit. Planet. Sci.* **52**, 1843-1858.

1152 Pourkhorsandi H., Gattacceca J., Devouard B., D’Orazio M., Rochette P., Beck P., Sonzogni C., and
1153 Valenzuela M. (2017b) The ungrouped chondrite El Médano 301 and its comparison with other
1154 reduced ordinary chondrites. *Geochim. Cosmochim. Acta* **218**, 98-113.

1155 Qin L., Alexander C. M. O., Carlson R. W., Horan M. F. and Yokoyama T. (2010) Contributors to
1156 chromium isotope variation of meteorites. *Geochim. Cosmochim. Acta* **74**, 1122–1145.

1157 Render J., Ebert S., Burkhardt C., Kleine T. and Brennecke G. A. (2019) Titanium isotopic evidence
1158 for a shared genetic heritage of refractory inclusions from different carbonaceous chondrites.
1159 *Geochim. Cosmochim. Acta* **254**, 40–53.

1160 Rochette P., Gattacceca J., Bonal L., Bourot-Denise M., Chevrier V., Clerc J.-P., Consolmagno G.,
1161 Folco L., Gounelle M., Kohout T., Pesonen L., Quirico E., Sagnotti L. and Skripnik A. (2008)
1162 Magnetic Classification of Stony Meteorites: 2. Non-Ordinary Chondrites, *Meteorit. Planet. Sci.* **43**,
1163 959-980.

1164 Sanborn M. E., Wimpenny J., Williams C. D., Yamakawa A., Amelin Y., Irving A. J. and Yin Q.-Z.
1165 (2019) Carbonaceous achondrites Northwest Africa 6704/6693: Milestones for early Solar System
1166 chronology and genealogy. *Geochim. Cosmochim. Acta* **245**, 577–596.

1167 Schrader D. L., Franchi I. A., Connolly H. C., Greenwood R. C., Lauretta D. S. and Gibson J. M.
1168 (2011) The formation and alteration of the Renazzo-like carbonaceous chondrites I: Implications of
1169 bulk-oxygen isotopic composition. *Geochim. Cosmochim. Acta* **75**, 308-325.

1170 Schrader D. L., Davidson J., Greenwood R. C.; Franchi I. A. and Gibson J. M. (2014) A water-ice rich
1171 minor body from the early Solar System: The CR chondrite parent asteroid. *Earth Planet. Sci. Lett.*
1172 **407**, 48-60.

1173 Scott E. R. D. and G. J. Taylor (1985) Petrology of types 4-6 carbonaceous chondrites. Proc. 15th
1174 Lunar Planet Sci. Conf., *JGR* **90**, Suppl., C699-C709.

1175 Schneider J. M., Burkhardt C., Marrocchi Y., Brennecke A. and Kleine T. (2020) Early evolution of the
1176 solar accretion disk inferred from Cr-Ti-O isotopes in individual chondrules. *Earth Planet. Sci. Lett.*
1177 (in press).

1178 Simon J. I., Cuzzi J. N., McCain K. A., Cato M. J., Christoffersen P. A., Fisher K. R., Srinivasan P.,
1179 Tait A. W., Olson D. M., Scargle J. D. (2018) Particle size distributions in chondritic meteorites:
1180 Evidence for pre-planetesimal histories. *Earth Planet. Sci. Lett.* **494**, 69-82.

1181 Smith D. L., Russell S. S., Gounelle M., Greenwood R. C. and Franchi I. A. (2004) NWA 1152 and
1182 Sahara 00182: New primitive carbonaceous chondrites with affinities to the CR and CV groups.
1183 *Meteorit. Planet. Sci.* **39**, 2009-2032.

1184 Starkey N. A., Jackson C. R. M., Greenwood R. C., Parman S., Franchi I. A., Jackson M., Fitton J. G.,
1185 Stuart F.M., Kurz M. and Larsen L.M. (2016). Triple oxygen isotopic composition of the high
1186 ³He/⁴He mantle. *Geochim. Cosmochim. Acta* **176**, 227-238.

1187 Stöffler D., Keil K. and Scott E. R. D. (1991) Shock metamorphism of ordinary chondrites. *Geochim.*
1188 *Cosmochim. Acta* **55**, 3845-3867.

- 1189 Stöffler, D., Hamann C. and Metzler K. (2018) Shock metamorphism of planetary silicate rocks and
 1190 sediments: Proposal for an updated classification system. *Meteorit. Planet. Sci.* **53**, 5-49.
- 1191 Stracke, A., Palme, H., Gellissen, M., Münker, C., Kleine, T., Birbaum, K., Günther, D., Bourdon, B.,
 1192 and Zipfel, J. 2012. Refractory element fractionation in the Allende meteorite: Implications for solar
 1193 nebula condensation and the chondritic composition of planetary bodies. *Geochim. Cosmochim.*
 1194 *Acta* **85**, 114–41.
- 1195 Teitler S.A., Paque J.M., Cuzzi J.N., and Hogan R.C. (2010) Statistical tests of chondrule sorting.
 1196 *Meteorit. Planet. Sci.* **45**, 1124–1135.
- 1197 Trinquier A., Birck J. and Allegre C. J. (2007) Widespread ⁵⁴Cr heterogeneity in the inner solar system.
 1198 *Astroph. J.* **655**, 1179–1185.
- 1199 Trinquier A., Elliott T., Ulfbeck D., Coath C., Krot A. N. and Bizzarro M. (2009) Origin of
 1200 nucleosynthetic isotope heterogeneity in the solar protoplanetary disk. *Science* **324**, 374–376.
- 1201 Ushikubo T., Kimura M., Kita N. T. and Valley J.W. (2011) Primordial oxygen isotope reservoirs of the
 1202 solar nebula recorded in chondrules in Acfer 094 carbonaceous chondrite. *Geochim. Cosmochim.*
 1203 *Acta* **90**, 242-264.
- 1204 Van Schmus W. R. (1969) Mineralogy, petrology and classification of types 3 and 4 carbonaceous
 1205 chondrites. In *Meteorite Research* (ed. P. M. Millman), pp. 480 -491. Reidel.
- 1206 Wang Z., Becker H. and Wombacher F. (2014) Mass fractions of S, Cu, Se, Mo, Ag, Cd, In, Te, Ba,
 1207 Sm, W, Tl and Bi in geological reference materials and selected carbonaceous chondrites
 1208 determined by isotope dilution ICP-MS. *Geostand. Geoanal. Res.* **39**, 185–208.
- 1209 Warren P. H. (2011) Stable isotopes and the noncarbonaceous derivation of ureilites, in common with
 1210 nearly all differentiated planetary materials. *Geochim. Cosmochim. Acta* **75**, 6912-6926.
- 1211 Weckwerth G. (2014) Instrumental neutron activation analyses of the most Earth-like meteorites. *J.*
 1212 *Radioanal. Nucl. Chem.* **299**, 221-228.
- 1213 Weckwerth G. and Weber D. (1998) The 3rd member of the Coolidge type grouplet: implications for
 1214 element fractionations trends in carbonaceous chondrites. In: *29th Lunar Planet Sci. Conf.*
 1215 (abstract # 1739).
- 1216 Weckwerth G., Wolf D., Bartoschewitz R. and Ackermann D. (2001) NWA 779, a new CV-chondrite
 1217 with relations to the Coolidge grouplet? In: *64th Ann. Meet. Meteorit. Soc.* (abstract #5378).
- 1218 Weisberg M. K. (2001) Sahara 00182, the first CR3 chondrite and formation of multi-layered
 1219 chondrules. *Meteorit. Planet. Sci.* **36**, A222–A223 (abstract).
- 1220 Weisberg M.K., Prinz M., Clayton R.N., and Mayeda T.K. (1997) CV3 chondrites: three subgroups, not
 1221 two. *Meteorit. Planet. Sci.* **32**, A138–A139 (abstract).
- 1222 Weisberg M. K., McCoy T. J. and Krot A. N. (2006) Systematics and evaluation of meteorite
 1223 classification. In *Meteorites and the early solar system II* (ed. D. S. Lauretta and H. Y. McSween
 1224 jr.), University of Arizona Press. pp. 679-712.
- 1225 Wlotzka F. (1993) A weathering scale for the ordinary chondrites (abstract). *Meteoritics* **28**, 460.
- 1226 Wolf D. and Palme, H. 2001. The solar system abundances of phosphorus and titanium and the
 1227 nebular volatility of phosphorus. *Meteoritics* **36**, 559–571.
- 1228 Wood B. J., Smythe D. J. and Harrison T. (2019) The condensation temperatures of the elements: A
 1229 reappraisal. *Am. Min.* **104**, 844-856.

- 1230 Wulf A. V., Palme H. and Jochum K. P. (1995) Fractionation of volatile elements in the early solar
1231 system: evidence from heating experiments on primitive meteorites. *Planet. Space Sci.* **43**, 451-
1232 468.
- 1233 Yamakawa A., Yamashita K. Makishima A. and Nakamura E. (2009) Chemical separation and mass
1234 spectrometry of Cr, Fe, Ni, Zn, and Cu in terrestrial and extraterrestrial material using thermal
1235 ionization mass spectrometry. *Anal Chem.* **81**, 23, 9787-9794.
- 1236 Young E. D. and Russell S. S. (1998) Oxygen reservoirs in the early solar nebula inferred from an
1237 Allende CAI. *Science* **282**, 1874–1877.
- 1238 Zhang J., Dauphas N., Davis A. M. and Pourmand A. (2011) A new method for MC-ICP-MS
1239 measurement of titanium isotopic composition: Identification of correlated isotope anomalies in
1240 meteorites. *J. Anal. At. Spectrom.* **26**, 2197.
- 1241 Zhang J., Dauphas N., Davis A. M., Leya I. and Fedkin A. (2012) The proto-Earth as a significant
1242 source of lunar material. *Nat. Geosci.* **5**, 251–255.
- 1243

1244

TABLES

1245 **Table 1:** Sample allocation, weight, and designation of the investigated (sub)samples of CL
1246 chondrites.

	Coolidge	Loongana 001	LoV 051	NWA 033	NWA 13400
Powder sample, total (mg)	559	565	513	598	610
ICP-MS					
University of Münster, Inst. f. Planetologie					
Sample powder (mg)	128	137	81	163	178
ICP-MS					
University of Münster, Inst. f. Mineralogie					
Sample powder (mg)	86	86	87	84	86
Laser fluorination					
Open University, Milton Keynes					
Sample powder (mg)	10	10	15	10	10
XRF					
University of Cologne					
Sample powder (mg)	131	130	130	134	135
SEM-EDX, Polarizing microscopy					
University of Münster, Inst. f. Planetologie					
Polished thin section numbers (size; mm ²)	-K-397-a-1 (52)	-F-a-1 (54)	-MS-a-1 (76)	PL-01047 (112)	-MS-a-1 (361)
LA-ICP-MS					
University of Münster, Inst. f. Mineralogie					
Thick section numbers (size; mm ²)	-K-397-a (52)	-F-a (44)	-MS-a (76)	-MS-a (126)	-MS-a (152)
Sample source	1	2	3	4	5

1247 1: University of Cologne, Inst. f. Geologie und Mineralogie, Germany; 2: Senckenberg Forschungsinstitut und Naturmuseum,
1248 Frankfurt, Germany; 3: CEREGE (CNRS/University Aix-Marseille), France; 4: University of Münster, Inst. f. Planetologie,
1249 Germany; 5: Mirko Graul, Bernau, Germany.

1250

1251 **Table 2:** Classification details for the investigated CL chondrites and modal abundances of their
1252 lithologic components.

	Coolidge	Loongana 001	LoV 051	NWA 033	NWA 13400
Proposed petrologic type ¹	4	4	3.9	4	3.9
PMD Fa ²	2.5	3.1	9.2	4.4	8.9
Shock stage ³	C-S2	C-S2	C-S2	C-S2	C-S2
Weathering grade ⁴	W2	W3	W1/2	W3/4	W2/3
Modal abundances (vol%)					
Chondrules + fragments	79	67	78	72	76
Inter-chondrule matrix	18	20	17	21	17
Inter-chondrule metal/sulfides ⁵	3	5	5	6	6
CAIs ⁶	0.1	8.0	0.4	0.9	1.0

1253 ¹ According to Hutchison (2004); ² PMD Fa: Percentage mean deviation (mol%) of fayalite values in olivine grains (see also
1254 Table 4); ³ according to Stöffler et al. (2018); ⁴ according to Wlotzka (1993); ⁵ partly/largely replaced by oxidation products;
1255 ⁶ Highly variable due to small thin section sizes (see Hezel et al., 2008).

1256

1257 **Table 3.** Magnetic properties of the investigated CL chondrites, compared to literature data for other
1258 groups of carbonaceous chondrites (CV_{red}, CV_{oxA}, CV_{oxB}, CR). χ : magnetic susceptibility; sd: standard
1259 deviation; M_S: saturation magnetization; M_{RS}: saturation remanent magnetization; B_C: coercive force;
1260 B_{CR}: remanent coercive force.

Meteorite	log χ	sd	n or studied mass (g)	M _S (Am ² /kg)	M _{RS} (Am ² /kg)	B _C (mT)	B _{CR} (mT)	M _{RS} /M _S	B _{CR} /B _C	n or studied mass (mg)
Coolidge	4.94		23.4 g							
Loongana 001	4.97		4.3 g							
LoV 051	5.24		15.0 g	32.3	0.50	3.08	18.8	1.55x10 ⁻²	6.10	205 mg
NWA 033	4.69		22.7 g							
CV _{red}	4.43	0.22	10	8.03±4.40	0.58±0.26	16.9±7.0	66.1±37.2	7.22x10 ⁻²	3.91	10
CV _{oxA}	3.62	0.27	11	0.69±0.37	0.053±0.018	15.4±0.6	64.6±12.1	7.68x10 ⁻²	4.19	11
CV _{oxB}	4.39	0.27	10	5.52±2.78	1.19±0.49	23.9±5.5	44.8±7.0	2.16x10 ⁻¹	1.87	10
CR	5.04	0.12	14	47.3	0.43	1.33	16.1	9.09x10 ⁻³	12.11	259 mg

1261 Susceptibility data for CV chondrites: Rochette et al. (2008) and Bonal et al. (2020) with the addition of Catalina 300 (CV_{oxB})
1262 from Gattacceca et al. (2020). Susceptibility data for CR chondrites, Loongana, and Coolidge: Rochette et al. (2008). M_S and
1263 M_{RS} data for CV chondrites: Bonal et al. (2020).

1264

1265 **Table 4.** Mean chemical composition of olivine in the investigated CL chondrites (EMPA; wt.%).

	Coolidge	Loongana 001	LoV 051	NWA 033	NWA 13400
SiO ₂	40.9±0.2	41.1±0.3	40.5±0.3	40.7±0.2	40.2±0.4
TiO ₂	0.07±0.05	0.06±0.04	0.04±0.04	0.05±0.03	0.03±0.03
Al ₂ O ₃	0.05±0.08	0.02±0.04	0.02±0.02	0.03±0.04	0.03±0.05
Cr ₂ O ₃	0.09±0.18	0.04±0.03	0.05±0.04	0.04±0.03	0.05±0.05
FeO	13.8±0.4	11.9±0.4	12.5±1.1	12.8±0.6	14.1±1.2
MnO	0.23±0.03	0.23±0.03	0.24±0.03	0.24±0.04	0.23±0.05
MgO	45.8±0.3	47.0±0.4	47.5±0.8	46.2±0.5	45.8±1.1
CaO	0.03±0.04	0.02±0.02	0.01±0.01	0.02±0.02	0.04±0.04
Na ₂ O	0.01±0.01	0.01±0.02	0.01±0.02	0.01±0.02	0.01±0.02
NiO	0.02±0.02	0.02±0.02	0.02±0.02	0.02±0.02	0.03±0.03
Total	101.00	100.40	100.89	100.11	100.52
<i>Fa</i>	14.5±0.4 (12.8-15.1)	12.5±0.4 (11.0-13.2)	12.8±1.2 (10.5-15.0)	13.5±0.6 (10.1-14.5)	14.7±1.3 (10.2-16.0)
<i>FeO/MnO</i>	60	52	52	53	61
<i>n</i>	44	49	47	46	30

1266 *Fa*: Fayalite content in olivine (mol%); ±: 1 standard deviation; Numbers in parenthesis: range of measured values.

1267

1268

1269 **Table 5.** Mean chemical composition of low-Ca pyroxene in the investigated CL chondrites (EMPA;
1270 wt.%).

	Coolidge	Loongana 001	LoV 051	NWA 033	NWA 13400
SiO ₂	58.5±0.7	58.2±0.8	57.6±0.7	58.4±0.9	58.0±1.0
TiO ₂	0.12±0.06	0.10±0.05	0.13±0.06	0.10±0.06	0.10±0.06
Al ₂ O ₃	0.81±0.25	0.59±0.23	0.67±0.24	0.73±0.30	0.71±0.16
Cr ₂ O ₃	0.37±0.11	0.33±0.07	0.32±0.07	0.39±0.09	0.40±0.07
FeO	6.37±2.59	6.99±1.40	6.99±2.26	5.32±2.04	4.51±2.55
MnO	0.14±0.08	0.16±0.05	0.16±0.08	0.13±0.06	0.12±0.05
MgO	34.2±1.8	33.5±0.9	34.2±1.6	34.6±1.4	35.7±1.5
CaO	0.48±0.07	0.44±0.15	0.57±0.16	0.45±0.12	0.55±0.05
Na ₂ O	0.01±0.01	0.01±0.01	0.01±0.02	0.02±0.02	0.02±0.02
NiO	0.02±0.04	0.05±0.05	0.03±0.02	0.04±0.03	0.09±0.08
Total	101.02	100.37	100.68	100.18	100.20
<i>Fs</i>	9.4±3.9 (1.3-14.1)	10.4±2.1 (6.9-14.0)	10.2±3.3 (2.7-14.6)	7.9±3.1 (3.1-15.2)	6.6±3.7 (1.2-15.9)
<i>Wo</i>	0.9±0.1 (0.7-1.2)	0.9±0.3 (0.5-1.5)	1.1±0.3 (0.7-1.9)	0.9±0.2 (0.4-1.3)	1.0±0.1 (0.8-1.2)
<i>FeO/MnO</i>	46	44	44	41	38
<i>n</i>	27	24	45	49	20

1271 *Fs*, *Wo*: Ferrosilite, wollastonite content in low-Ca pyroxene (mol%); ±: 1 standard deviation; Numbers in parenthesis: range of
1272 measured values.

1273

1274

1275 **Table 6.** Mean chemical composition of Ca-rich pyroxene in the investigated CL chondrites (EMPA;
1276 wt.%).

	Coolidge	Loongana 001	LoV 051	NWA 033	NWA 13400
SiO ₂	54.6±1.1	54.2±2.1	53.7±1.2	53.9±0.7	54.3±0.9
TiO ₂	1.09±0.33	0.93±0.48	0.96±0.31	1.07±0.29	1.06±0.38
Al ₂ O ₃	2.75±1.15	3.91±2.40	3.38±1.40	3.33±1.32	2.91±0.89
Cr ₂ O ₃	0.69±0.16	0.84±0.46	0.69±0.22	0.98±0.31	0.59±0.14
FeO	4.12±1.97	3.40±2.03	3.42±1.80	2.95±1.36	2.64±1.85
MnO	0.21±0.05	0.22±0.10	0.17±0.04	0.23±0.08	0.16±0.05
MgO	21.0±2.5	22.2±4.5	20.6±2.2	19.4±1.6	23.1±3.4
CaO	16.3±4.2	14.7±6.1	17.3±3.6	18.4±2.6	15.2±4.4
Na ₂ O	0.30±0.14	0.19±0.14	0.29±0.18	0.33±0.23	0.09±0.12
NiO	0.03±0.04	0.04±0.07	0.03±0.04	0.04±0.04	0.07±0.05
Total	101.09	100.63	100.54	100.63	100.12
<i>Fs</i>	6.6±3.2 (1.4-10.8)	5.4±3.1 (1.6-9.8)	5.5±2.9 (1.4-12.0)	4.8±2.2 (0.7-8.6)	4.2±2.9 (0.8-10.2)
<i>Wo</i>	33.5±8.8 (18.4-43.6)	30.9±13.5 (12.3-43.7)	35.5±7.6 (16.3-45.6)	38.6±5.4 (27.1-49.3)	30.9±9.4 (10.7-44.6)
<i>FeO/MnO</i>	20	15	20	13	17
<i>n</i>	10	8	38	28	23

1277 *Fs*, *Wo*: Ferrosilite, wollastonite content in Ca-rich pyroxene (mol%); ±: 1 standard deviation; Numbers in parenthesis: range of
1278 measured values.

1279 **Table 7.** Statistics (μm) for the distributions of apparent chondrule sizes in the investigated CL
 1280 chondrites, Allende (CV), and NWA 7020 (CR).

	Coolidge	Loongana 001	LoV 051	NWA 033	NWA 13400	Allende	NWA 7020
Mean	404 (610) ¹	414 (700) ¹	476	455	477	470	633
Median	270	288	403	332	342	357	506
StDev ²	405	347	327	349	421	366	468
Skewness	2.60	2.13	2.07	1.69	2.02	2.10	1.20
Min ³	55	75	75	65	50	70	65
Max ⁴	2790	2295	2490	2070	2930	2670	2540
n ⁵	145	235	397	274	512	421	148

1281 ¹ Literature data (Kallemeyn and Rubin, 1995); ² Standard deviation; ³ Size of the smallest chondrule; ⁴ Size of the largest
 1282 chondrule; ⁵ Number of analyzed chondrules.

1283

1284

1285 **Table 8.** Bulk composition of inter-chondrule matrix in the investigated CL chondrites (EMPA¹; wt.%).
 1286 Literature values for other carbonaceous groups are given for comparison. Clg: Coolidge; Loo:
 1287 Loongana; LoV: LoV051; 033: NWA 033; 13400: NWA 13400.

	CL					Mean CL	CV _{red} ²	CV _{oxA} ²	CV _{oxB} ²	CK	CR
	Clg	Loo	LoV	033	13400		Vigarano*	Allende*	Bali**	Karoonda*	Renazzo*
SiO ₂	30.8	27.7	30.9	29.5	32.8	30.3	31.2	30.1	32.2	34.1	36.6
TiO ₂	0.10	0.13	0.13	0.11	0.18	0.13	0.10	0.10	0.07	0.55	0.08
Al ₂ O ₃	2.01	2.18	1.56	2.04	1.41	1.84	4.70	2.48	2.04	7.63	3.10
Cr ₂ O ₃	0.79	0.81	0.44	0.61	0.89	0.71	0.44	0.41	0.35	0.40	0.41
FeO	31.5	34.5	30.3	32.3	25.2	30.8	35.9	34.3	36.7	28.14	28.3
MnO	0.14	0.15	0.16	0.15	0.20	0.16	0.15	0.23	0.25	0.14	0.38
MgO	28.3	25.6	28.9	27.5	31.3	28.3	18.8	21.7	18.2	18.7	18.4
CaO	0.97	1.61	1.11	1.23	0.98	1.18	1.68	2.55	3.34	3.98	1.01
Na ₂ O	0.25	0.29	0.36	0.53	0.09	0.30	0.54	0.24	0.54	0.22	1.35
K ₂ O	0.03	0.03	0.03	0.04	0.03	0.03	0.06	0.01	nd	0.13	0.19
P ₂ O ₅	0.15	0.19	0.13	0.16	0.24	0.17	nd	nd	nd	nd	nd
Ni	1.01	1.56	1.04	1.26	0.87	1.15	1.20	1.55	1.11	0.22	1.36
S	0.15	0.09	0.35	0.08	0.04	0.14	0.22	1.22	nd	0.09	3.72
Total	96.20	94.84	95.41	95.51	94.23	95.24	95.00	95.00	94.80	95.00	95.00
n	10	10	10	12	10		20	20	70	20	20

1288 ¹ defocused beam (30 μm)

1289 ² CV subgroups: CV_{red} = reduced; CV_{oxA} = oxidized Allende-type; CV_{oxB} = oxidized Bali-type (Weisberg et al., 1997)

1290 *McSween and Richardson (1977); recalculated to 95.00 wt.% for comparison

1291 **Unpublished data (Friend, pers. communication)

1292 nd: not determined

1293 n: number of analyzed areas

1294

1295 **Table 9.** Bulk chemical composition (major and minor elements; wt.%) of the investigated CL
 1296 chondrites and Allende. Literature data for Allende are given for comparison.

	Lab ¹	RSD (%) ²	Coolidge ³	Loongana 001 ⁴	LoV 051	NWA 033	NWA 13400	Allende ⁵
SiO ₂	A	< 1	33.05 (33.59; 33.52; nd)	34.64	33.94	34.36	34.26	34.05 (34.3; 34.15; nd)
TiO ₂	A	< 1	0.14 (0.14; 0.14; nd)	0.15	0.15	0.15	0.15	0.15 (0.15; 0.15, 0.13)
Al ₂ O ₃	A	< 1	3.15 (2.83; 2.83; 3.74)	2.91 (3.36)	3.20	3.07	3.11	3.20 (3.28; 3.23, 3.15)
Cr ₂ O ₃	A	< 1	0.51 ⁶ (0.46; 0.43; 0.64)	0.49 (0.53)	0.51	0.52	0.52	0.50 (0.53; 0.53; 0.53)
FeO	A	< 1	30.99 (27.02; 27.04; 24.83)	29.83 (29.46)	30.46	29.02	30.07	29.82 (30.3; 30.31; 30.60)
MnO	A; B	< 1; 1.3	0.15; 0.15 (0.14; 0.14; 0.15)	0.16; 0.16 (0.14)	0.14; 0.15	0.16; 0.15	0.15; 0.15	0.19; 0.19 (0.19; 0.19; 0.19)
MgO	A	< 1	24.52 (24.58; 24.57; 24.87)	25.32 (24.04)	25.30	25.39	24.47	24.83 (24.6; 24.56; 24.79)
CaO	A	< 1	2.13 (2.06; 2.06; 2.74)	2.09 (2.46)	2.84	2.47	2.17	2.48 (2.58; 2.61; 2.49)
Na ₂ O	A	< 1	0.32 (nd; 0.24; 0.26)	0.20 (0.22)	0.27	0.27	0.18	0.49 (0.46; nd; 0.43)
K ₂ O	A	< 1	0.02 (nd; 0.04; 0.02)	0.02 (0.02)	0.01	0.02	0.01	0.03 (0.04; nd; 0.03)
P ₂ O ₅	A	< 1	0.24 (0.18; nd; nd)	0.23	0.22	0.25	0.25	0.25 (0.24; 0.24; 0.24)
Co	B	4.2	0.060 (0.08; 0.06; 0.06)	0.057 (0.06)	0.058	0.056	0.061	0.061 (0.06; 0.068; 0.066)
Ni	A	< 1	1.39 (1.13; 1.20; nd)	1.30	1.31	1.28	1.28	1.33 (1.42; 1.39*; 1.42)
S ⁷	C	-	2.1 (nd; nd; nd)	0.7	0.5	0.5	0.9	2.1 (2.10; nd; 2.08)
Total			98.98	98.10	98.91	97.52	97.58	99.49

1297 ¹ Analytical method, laboratory: A: XRF, Institut für Geologie und Mineralogie, University of Cologne; B: ICP-MS, Institut für
 1298 Mineralogie, University of Münster; C: SEM-EDX, Institut für Planetologie, University of Münster

1299 ² Relative standard deviation of measured values in %

1300 ³ Literature data (Wolf and Palme, 2001; Weckwerth, 2014; Kallemeyn and Rubin, 1995) in parenthesis. nd: not determined

1301 ⁴ Literature data (Kallemeyn and Rubin, 1995) in parenthesis

1302 ⁵ Literature data (Jarosewich et al., 1987; Stracke et al., 2012, average of 39 samples; Braukmüller et al., 2018) in parenthesis.

1303 * XRF/ICP-MS average.

1304 ⁶ Mean of literature values; own value (0.72 wt.%) probably biased by unknown contamination

1305 ⁷ Rough estimate; recalculated values relative to Allende (SEM-EDX; see section 3.2.1)

1306

1307 **Table 10.** Bulk chemical composition of the investigated samples (trace elements; ppm). Numbers in
 1308 italics indicate values that show evidence for modification by terrestrial weathering.

	Lab ¹	RSD ² (%)	Coolidge ³	Loongana 001 ⁴	LoV 051	NWA 033	NWA 13400	Allende	Allende (Literature) ⁵		
									Stra	Brauk	Others
Li	B	1.7	<i>2.10</i>	<i>2.13</i>	<i>2.07</i>	<i>2.10</i>	<i>1.97</i>	1.69			1.81 ^a ; 1.64 ^b
Sc	D	4.9	15.5 (12.0; 9.4)	10.5 (11.2)	15.3	10.6	11.5	11.8			11.3 ^a ; 10.8 ^b ; 10.7 ^c
V	B	2.2	85.6 (106; 91)	73.3 (102)	85.5	81.4	81.6	95.9	90.2 ^f	92.6	95.2 ^a ; 91 ^b ; 91 ^c
Zn	A	< 1	56.7 (60; 33)	33.7 (50)	32.5	43.5	51.6	102	106	123	119 ^a ; 118 ^d
Se	D	32	5.05 (3.2; 3.2)	5.78 (3.3)	2.62	5.18	3.04	9.57			9.21 ^d ; 8.25 ^e
Rb	B	2.3	0.29	0.92	0.42	0.50	0.18	1.21	1.32	1.15	1.18 ^a ; 1.17 ^b
Sr	B	0.6	14.8	15.3	18.8	24.2	15.5	14.6	15.7		15.6 ^a ; 15.6 ^c
Y	B	1.2	2.66	3.75	2.81	3.77	2.48	2.60	2.63		2.88 ^a ; 2.77 ^b
Zr	B	0.7	6.82	8.89	7.40	9.15	6.20	6.60	6.77	6.45	6.61 ^a ; 7.1 ^b
Nb	B	2.4	0.519	0.620	0.662	0.574	0.535	0.531	0.569	0.503	0.573 ^a ; 0.58 ^b
Mo	B	0.2	1.52	1.50	1.64	1.40	1.57	1.51	1.45		1.64 ^a ; 1.44 ^f
Te	D	8.6	0.781	0.575	0.528	0.588	0.611	1.21		1.04	0.94 ^e
Cs	B	2.8	0.024	0.060	0.042	0.044	0.011	0.088	0.098	0.080	0.086 ^b
Ba	B	0.3	33.9	15.2	13.0	61.6	73.3	4.49	4.74	4.21	4.53 ^a ; 4.6 ^b ; 4.7 ^c
La	B	0.2	0.642 (0.505; 0.89)	1.482	0.527	0.959	0.461	0.487	0.490	0.471	0.516 ^a ; 0.498 ^b
Ce	B	0.1	1.400	3.114	1.318	2.148	1.152	1.24	1.24	1.21	1.29 ^a ; 1.29 ^b
Pr	B	0.6	0.228	0.459	0.201	0.316	0.179	0.193	0.192	0.191	0.201 ^a ; 0.195 ^b
Nd	B	0.4	1.116	2.006	1.006	1.515	0.891	0.975	0.967	0.998	1.02 ^a ; 0.989 ^d
Sm	B	0.2	0.335 (0.311; 0.34)	0.506	0.324	0.427	0.283	0.316	0.313	0.328	0.329 ^a ; 0.310 ^b ; 0.331 ^e
Eu	B	0.4	0.115 (0.118; 0.12)	0.153	0.117	0.139	0.109	0.111	0.115	0.110	0.114 ^a ; 0.108 ^b
Gd	B	0.1	0.404	0.596	0.407	0.530	0.364	0.397	0.401	0.439	0.417 ^a ; 0.409 ^b
Tb	B	0.2	0.074	0.102	0.074	0.091	0.067	0.073	0.072	0.074	0.076 ^a ; 0.073 ^b
Dy	B	0.4	0.482	0.661	0.496	0.582	0.441	0.479	0.479	0.499	0.508 ^a ; 0.483 ^b
Ho	B	0.1	0.107	0.150	0.110	0.133	0.098	0.104	0.100		0.107 ^a ; 0.103 ^b
Er	B	0.4	0.309	0.432	0.318	0.403	0.287	0.300	0.299	0.304	0.310 ^a ; 0.305 ^b
Tm	B	0.8	0.054	0.057	0.053	0.057	0.048	0.054	0.053	0.053	0.056 ^a ; 0.050 ^b
Yb	B	0.1	0.317 (0.329; 0.3)	0.360 (0.338)	0.343	0.345	0.305	0.326	0.319	0.327	0.325 ^a ; 0.302 ^b
Lu	B	1.8	0.046 (0.052; 0.04)	0.062	0.048	0.061	0.043	0.044	0.046	0.047	0.046 ^a ; 0.046 ^b
Hf	B	2.6	0.203 (nd; 0.25)	0.264	0.206	0.262	0.178	0.192	0.188	0.191	0.202 ^a ; 0.199 ^b
Ta	B	0.1	0.030	0.037	0.032	0.032	0.028	0.033	0.033		0.034 ^a ; 0.041 ^b
Tl	B	10	0.004	0.022	0.006	0.064	0.007	0.071		0.062	0.059 ^e
Pb	B	0.6	0.325	0.635	0.196	0.508	0.183	1.29	1.52	1.08	1.27 ^a ; 1.25 ^b
Th	B	3.9	0.080	0.315	0.076	0.106	0.072	0.084	0.078	0.056	0.059 ^a ; 0.082 ^b
U	B	4.1	0.037	0.041	0.028	0.100	0.031	0.015	0.017	0.013	0.015 ^a ; 0.018 ^b

1309 ¹ Analytical method and laboratory: A: XRF, Institut für Geologie und Mineralogie, University of Cologne; B: ICP-MS, Institut für
 1310 Mineralogie, University of Münster, Germany; D: LA-ICP-MS, Institut für Mineralogie, University of Münster.
 1311 ³ Literature data (Kallemeyn and Rubin, 1995; Weckwerth, 2014) in parenthesis; nd: not determined
 1312 ⁴ Literature data (Kallemeyn and Rubin, 1995) in parenthesis
 1313 ⁵ Literature data for Allende. Averaged values are shown in Figs. 9-10. Stra: Stracke et al. (2012; average of 39 subsamples; *
 1314 XRF/ICP-MS average). Brauk: Braukmüller et al. (2018; Smithsonian standard). Others: ^a Barrat et al. (2012); ^b Pourkhorsandi et
 1315 al. (2017b); ^c Greenwood et al. (2010); ^d Hezel and Palme (2008); ^e Wang et al. (2014); ^f Burkhardt et al. (2014).
 1316

1317 **Table 11.** Bulk O isotopic composition of the investigated CL chondrites.

	Coolidge	Loongana 001	LoV 051	NWA 033	NWA 13400
$\delta^{17}\text{O} \pm 1\sigma$ (‰)*	-6.835 ± 0.216	-4.781 ± 0.170	-7.626 ± 0.486	-3.911 ± 0.164	-4.017 ± 0.023
$\delta^{18}\text{O} \pm 1\sigma$ (‰)*	-3.336 ± 0.169	-1.035 ± 0.136	-4.151 ± 0.518	0.102 ± 0.228	-0.021 ± 0.007
$\Delta^{17}\text{O} \pm 1\sigma$ (‰)*	-5.101 ± 0.128	-4.243 ± 0.099	-5.467 ± 0.216	-3.964 ± 0.046	-4.006 ± 0.026

1318 Mean of 2 measurements, each. \pm : 1 standard deviation

1319

1320

1321 **Table 12.** Bulk Ti and Cr isotopic composition of the investigated CL chondrites and Allende.

	N [Ti]	$\epsilon^{46}\text{Ti} \pm 2\sigma$	$\epsilon^{48}\text{Ti} \pm 2\sigma$	$\epsilon^{50}\text{Ti} \pm 2\sigma$	N [Cr]	$\epsilon^{53}\text{Cr} \pm 2\sigma$	$\epsilon^{54}\text{Cr} \pm 2\sigma$
Coolidge	10	0.50 ± 0.09	0.07 ± 0.10	2.63 ± 0.10	8	0.07 ± 0.08	0.81 ± 0.10
Loongana 001	10	0.43 ± 0.13	-0.07 ± 0.07	2.57 ± 0.09	11	0.06 ± 0.08	0.68 ± 0.18
LoV 051	10	0.52 ± 0.06	-0.05 ± 0.04	2.85 ± 0.08	8	0.05 ± 0.07	0.76 ± 0.12
NWA 033	10	0.44 ± 0.10	-0.08 ± 0.09	2.35 ± 0.05	12	0.05 ± 0.11	0.64 ± 0.12
NWA 13400	10	0.53 ± 0.06	-0.05 ± 0.03	2.60 ± 0.07	9	0.14 ± 0.13	0.70 ± 0.13
Average CL		0.48 ± 0.04	-0.03 ± 0.03	2.60 ± 0.05		0.07 ± 0.04	0.71 ± 0.06
Allende	12	0.70 ± 0.06	-0.06 ± 0.04	3.21 ± 0.11	6 [*]	$0.12 \pm 0.12^*$	$0.96 \pm 0.22^*$
					4 [*]	$0.11 \pm 0.10^*$	$1.06 \pm 0.30^*$

1322 All reported uncertainties are Student-t 95% confidence intervals (95% CI). N: Number of analyses of the same solution.

1323 * Schneider et al. (2020)

1324

FIGURE CAPTIONS

1325
1326
1327
1328
1329
1330
1331
1332
1333
1334
1335
1336
1337
1338
1339
1340
1341
1342
1343
1344
1345
1346
1347
1348
1349
1350
1351
1352
1353
1354
1355
1356
1357
1358
1359
1360
1361
1362
1363
1364
1365

Fig. 1. Overall texture and lithologic components of the Loongana 001 meteorite as an example for the proposed CL group of carbonaceous chondrites (a: back-scatter electron image; b: phase map including color coding). Beside the omnipresent metal-rich porphyritic type-I chondrules (PO, POP) with irregular shapes (1), the following components are visible: 2) Barred olivine (BO) chondrule; 3) Al-rich chondrule; 4) Chondrule fragment; 5) Irregularly shaped chondrule adhering to a larger one; 6) Chondrule with thick pyroxene rim (7) and olivine-rich core; 8) Ca-Al-rich inclusion (CAI).

Fig. 2. Frequency distributions of fayalite (Fa) values (a) and ferrosilite (Fs) values (b) in olivine and low-Ca pyroxene, respectively, in CL chondrites. Coolidge, Loongana, and NWA 033 show narrow Fa distributions. The samples LoV 051 and NWA 13400 show broader distributions, indicating a less intensive metamorphic overprint.

Fig. 3. Chondrule textures in CL chondrites. a) Typical porphyritic olivine-pyroxene (POP) chondrule with irregular and lobate outline (Coolidge). b) Chondrule with several protuberances in NWA 13400. c) Assortment of differently sized and irregularly shaped chondrules or melt shreds (NWA 13400). d) Extreme complex chondrule (white outline), consisting of a porphyritic olivine (PO) chondrule core with irregular layers of adhering smaller chondrules or melt shreds, stacked on top of each other. The central chondrule is separated from these layers by an Fe-Ni layer (white). e) Layered olivine chondrule with concentric inner Fe-Ni layer and thin pyroxene rim (LoV 051). f) Multi-layered olivine chondrule with two cocentric inner Fe-Ni layers and an outer Fe-Ni layer (NWA 13400). g) Al-rich chondrule with fine-grained quench texture and large Al-rich enstatite crystals (dark gray; Loongana). h) Barred olivine (BO) chondrule of chemical type II with igneous rim in NWA 13400. SEM-BSE images; dark gray: low-Ca pyroxene; medium gray: olivine; white to light gray: Fe-Ni metal, sulfides; white to light gray linear features are terrestrial oxidation products along cracks (SEM-BSE images).

Fig. 4. Opaque phases in CL chondrites. a) Polycrystalline kamacite grain in a Coolidge chondrule, showing taenite exsolutions (light gray) and exsolutions of chromite and merrillite (black dots) along kamacite grain boundaries; b) Rare side-by-side occurrence of isolated kamacite (right center) and taenite grains (left center) in a chondrule in NWA 033. Other grains are FeS; c) Intergrowth texture of sulfide (FeS; gray) and kamacite (white) in a LoV chondrule; d) Very large polycrystalline FeS grain in a Coolidge chondrule; white: kamacite. (SEM-BSE images).

Fig. 5. Frequency distributions of apparent chondrule sizes (100 μm binning), measured on BSE photomosaics. a) Frequency distributions in the investigated CL chondrites; b) Average distribution in CL chondrites (blue solid line, calculated from data in a). Frequency distributions for the CV chondrites Allende (CV_{oxA}, red dashed line) and the CR chondrite NWA 7020 (black dotted line), obtained in this study, are shown for comparison. Please note the different scaling of the size axes in a) and b). n: number of measured chondrules.

1366 **Fig. 6.** Textures and components of refractory inclusions in CL chondrites. a) Complex CAI in
1367 Loongana, consisting of fine-grained subunits (anorthite, spinel) which are rimmed by Ca-rich
1368 pyroxene (medium gray), and some FeS (white); b) CAI in NWA 13400, mainly consisting of
1369 subhedral-euhedral spinel (medium-dark gray), FeS (white), partly surrounded by a spinel rim; c) CAI
1370 in Coolidge, rimmed by a spinel and diopside layer, probably a former Wark-Lovering rim. This
1371 inclusion contains a mineral assemblage consisting of FeS, TiO₂, and spinel, embedded in extremely
1372 fine-grained groundmass; d) Cl-apatite in a CAI in NWA 13400 (left center, light gray); e) Refractory
1373 metal nugget (light gray to white; rich in Os, Ir, Pt, Ru) in a CAI in Loongana; f) Amoeboid olivine
1374 aggregate (AOA) in LoV, intermingled with CAI material (right part of the inclusion). White to light-gray
1375 linear features in the images are terrestrial oxidation products along cracks (SEM-BSE images).

1376
1377 **Fig. 7.** Inter-chondrule matrix in CL chondrites. a) Overview of Loongana matrix, showing chondrule
1378 and mineral fragments (mostly olivine and low-Ca pyroxene), embedded in a fine-grained groundmass
1379 of very small grains of olivine and low-Ca pyroxene, with interstitial oxidation products of metals and
1380 sulfides. Microtextures of inter-chondrule matrix are shown for the CL chondrites Loongana (b),
1381 Coolidge (c), LoV 051 (d), NWA 033 (e), and NWA 13400 (f). The size distributions are bimodal with a
1382 coarser-grained fragment population, cemented by a finer-grained groundmass. The latter possibly
1383 crystallized during thermal metamorphism. Black to medium gray: silicates (olivine and pyroxene); light
1384 gray to white: oxidation products of metals and sulfides (SEM-BSE images).

1385
1386 **Fig. 8.** Bulk chemical compositions of CL chondrites (encircled red filled circles) and other groups of
1387 carbonaceous chondrites (CI, CM, CO, CV, CR, CK4; literature data). a) Al₂O₃ vs. MnO
1388 concentrations; the volatile lithophile element Mn is considerably depleted in CL chondrites compared
1389 to the other groups; the Al₂O₃ concentrations are in the range of CV and CK chondrites. b) Al₂O₃ vs.
1390 Zn concentrations; the CL chondrites show, on average, the lowest Zn concentrations among all major
1391 carbonaceous chondrite groups. c) Zr vs. Rb concentrations; CL chondrites show a characteristic
1392 combination of low Rb and high Zr concentrations. Literature data: CI (Lodders et al., 2009); Others
1393 (mean values, where possible): Kallemeyn and Wasson (1981, 1982); Jarosewich et al. (1987);
1394 Kallemeyn et al. (1991, 1994); Wolf and Palme (2001); Jarosewich (2006); Greenwood et al. (2010);
1395 Braukmüller et al. (2018).

1396
1397 **Fig. 9.** Cl-normalized (Lodders et al, 2009) lithophile element concentrations in CL chondrites and
1398 other carbonaceous chondrite groups. Elements are arranged in the order of increasing volatility
1399 (Wood et al. 2019). a) Data for CL chondrites (colored curves, circles) and Allende (black curve,
1400 squares), together with Allende literature data (dashed curve; see [Tables 9-10](#)). The volatile lithophile
1401 elements Mn, Na, K, Rb, and Cs are moderately to strongly depleted compared to Allende. b) Mean
1402 concentrations in the CL chondrites (red solid curve, filled circles) and other carbonaceous chondrite
1403 groups (CM, CO, CV, CR, CK4; literature values; black curves). The CL-trend of volatile element
1404 depletion and enrichment of other elements is evident. Literature data (mean values, where possible):
1405 Knab (1981); Kallemeyn and Wasson (1981); Jarosewich et al. (1987); Kallemeyn et al. (1991, 1994);

1406 Wolf and Palme (2001); Jarosewich (2006); Greenwood et al. (2010); McCoy-West et al. (2017);
1407 Braukmüller et al. (2018).

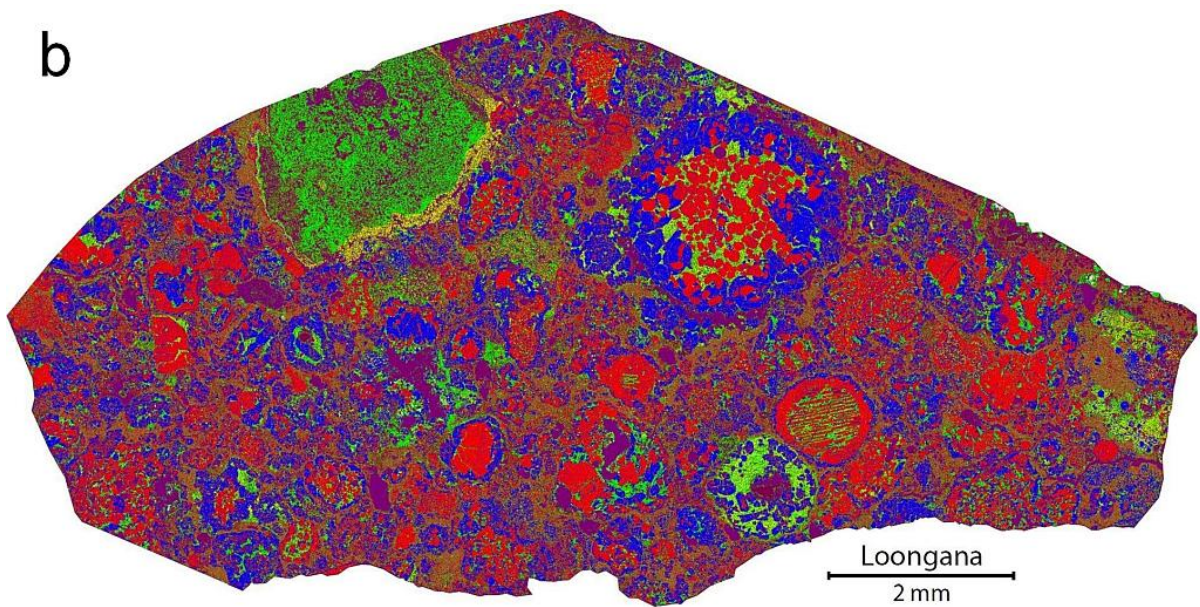
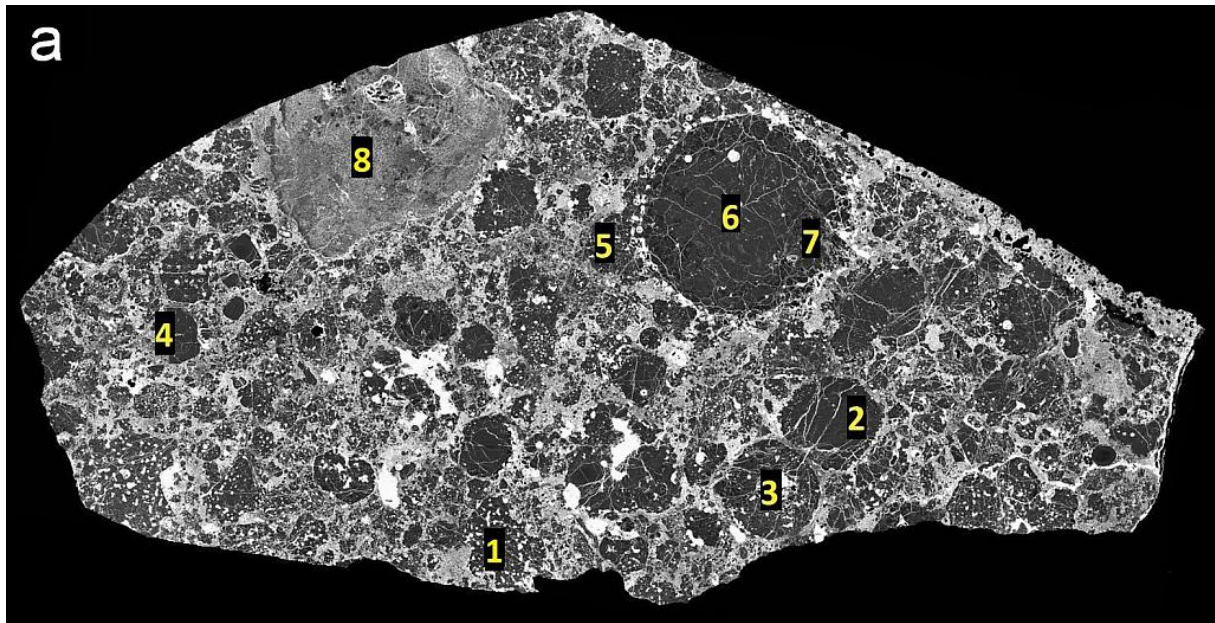
1408
1409 **Fig. 10.** CI-normalized (Lodders et al., 2009) concentrations of siderophile and chalcophile elements in
1410 CL chondrites and other carbonaceous chondrite groups. Elements are arranged in the order of
1411 increasing volatility (Wood et al. 2019). a) Data for CL chondrites (colored curves, circles) and Allende
1412 (black curve, squares), together with Allende literature data (dashed curve; see Tables 9-10). b) Mean
1413 concentrations in the CL chondrites (red curve, filled circles) and other carbonaceous chondrite groups
1414 (CM, CO, CV, CR, CK4; literature values; black curves). The concentrations of siderophile elements in
1415 CL chondrites are in the range of those in the other groups, with the highest value for the most
1416 refractory element (Mo). The concentrations of chalcophile elements in CL chondrites are the lowest of
1417 all other groups. Literature data (mean values, where possible): Matza and Lipschutz (1977; Ti in the
1418 Karoonda CK chondrite); Kallemeyn and Wasson (1981); Palme and Rammensee (1981); Jarosewich
1419 et al. (1987); Bischoff et al. (1993; Mo in the Acfer 059/EI Djouf 001 CR chondrite); Kallemeyn et al.
1420 (1991, 1994); Wolf and Palme (2001); Jarosewich (2006); Greenwood et al. (2010); Burkhardt et al.
1421 (2014; Mo in the Karoonda CK chondrite); Braukmüller et al. (2018).

1422
1423 **Fig. 11.** Bulk oxygen isotopic compositions of CL chondrites (red squares). Data fields for CO3
1424 (Alexander et al., 2018), CV3 and CK (Greenwood et al., 2010), and CR chondrites (Schrader et al.,
1425 2011, 2014) are shown for comparison. All samples plot on or slightly to the side of the Carbonaceous
1426 Chondrite Anhydrous Mineral (CCAM) line (Clayton and Mayeda, 1999). Other reference lines:
1427 Primitive Chondrule Minerals line (PCM) (Ushikubo et al., 2011); Young and Russell line (Y&R)
1428 (Young and Russell, 1998), Terrestrial Fractionation Line (TFL) are shown for comparison. Three of
1429 the samples plot within the fields of CV3 and CK chondrites, together with Allende (this study). The
1430 meteorites Coolidge and LoV 051 plot outside these fields and are characterized by a lower
1431 concentration of ^{17}O and ^{18}O .

1432
1433 **Fig. 12.** Bulk isotopic compositions of CL chondrites (filled circles; red). a) $\epsilon^{54}\text{Cr}$ vs. $\Delta^{17}\text{O}$; b) $\epsilon^{54}\text{Cr}$ vs.
1434 $\epsilon^{50}\text{Ti}$. Mean values for other chondrite groups are shown for comparison (open diamonds:
1435 carbonaceous chondrites; open circles and squares: non-carbonaceous chondrites). All carbonaceous
1436 chondrites (including CL chondrites) exhibit negative $\Delta^{17}\text{O}$ values and coupled $\epsilon^{50}\text{Ti}$ - $\epsilon^{54}\text{Cr}$
1437 excesses. The data for CL chondrites form a tight cluster at a unique position in the $\epsilon^{54}\text{Cr}$ - $\epsilon^{50}\text{Ti}$
1438 diagram, indicating their distinctness to the other groups. All reported uncertainties are Student-t 95%
1439 confidence intervals (95% CI). The chondrite groups are shown as composite points averaging
1440 multiple samples within each group. Literature data for Cr and Ti isotopes: Burkhardt et al. (2019);
1441 Mougél et al. (2018); Sanborn et al. (2019). Literature data for O isotopes: Clayton and Mayeda
1442 (1999), Dauphas and Schauble (2016), Burkhardt et al. (2017).

1443

FIGURES



Olivine
Low-Ca pyroxene
Ca-rich pyroxene

Al-rich material (CAIs, chondrule mesostasis)
Metals, sulfides
Interchondrule matrix

Fig. 1

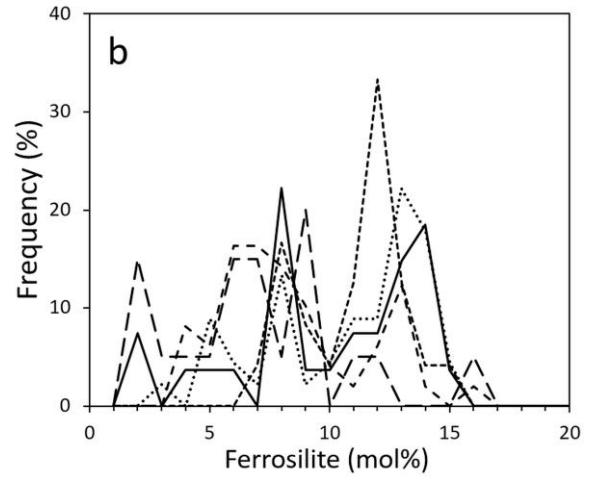
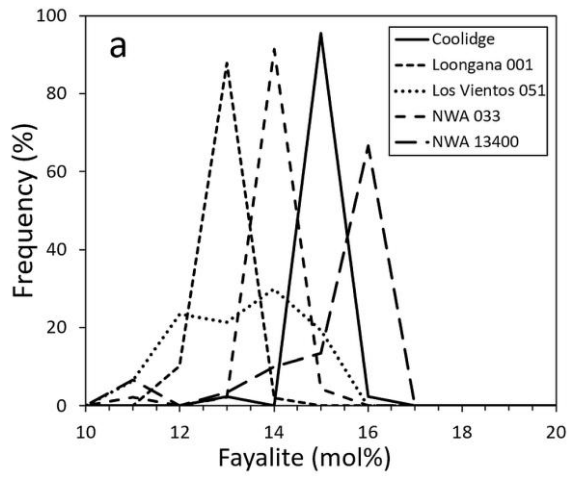


Fig. 2

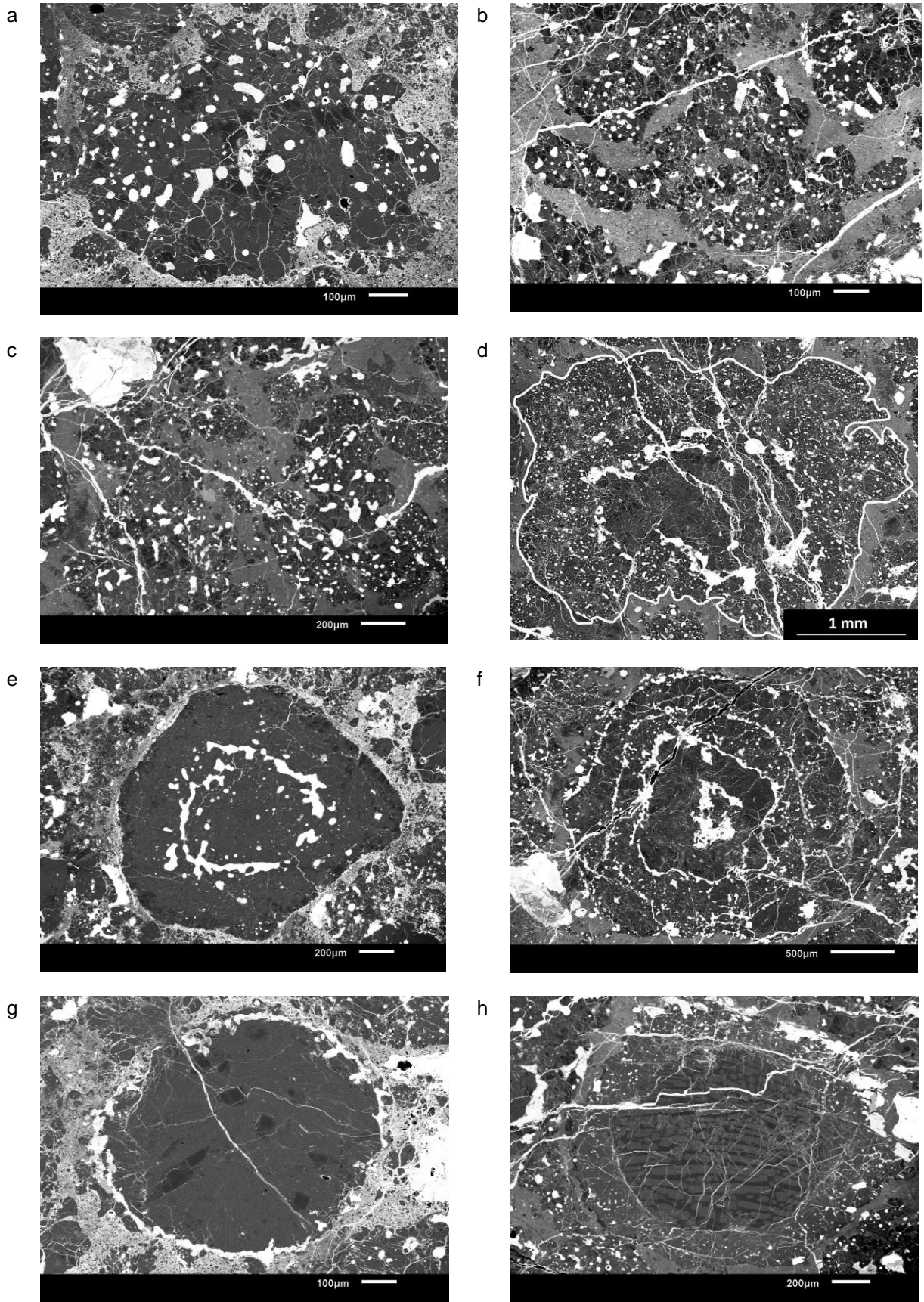


Fig. 3

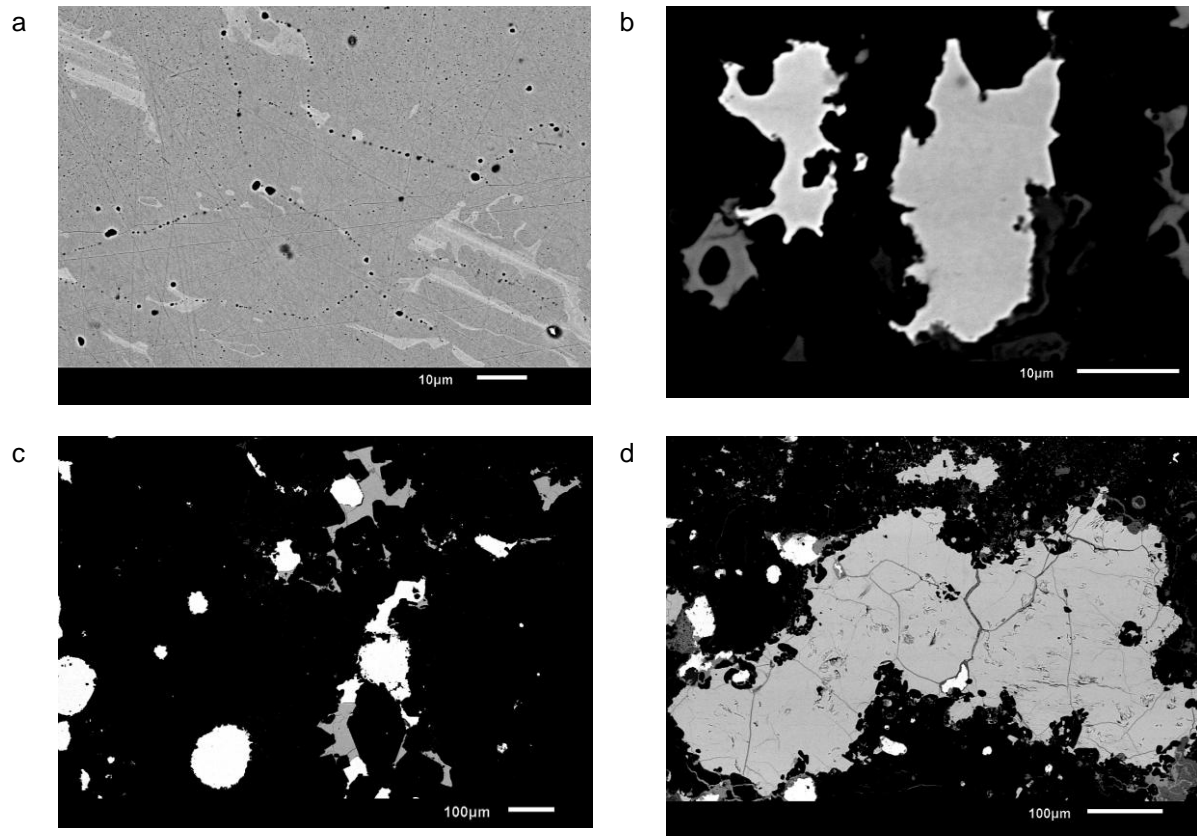


Fig. 4

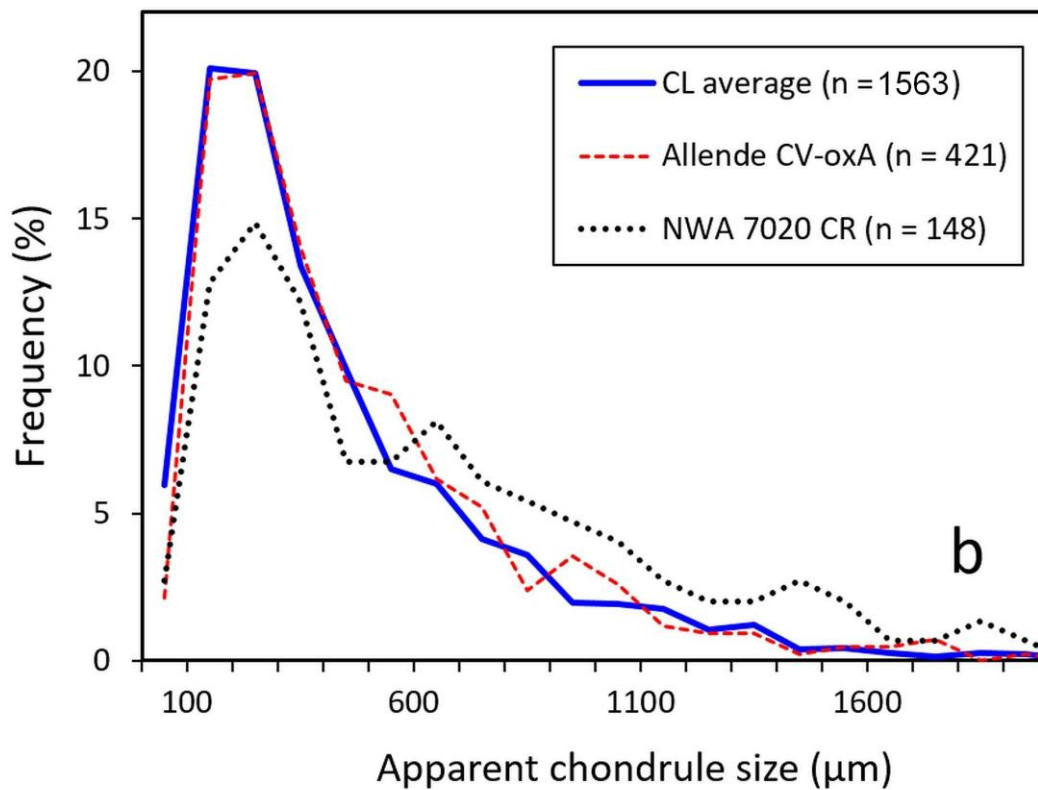
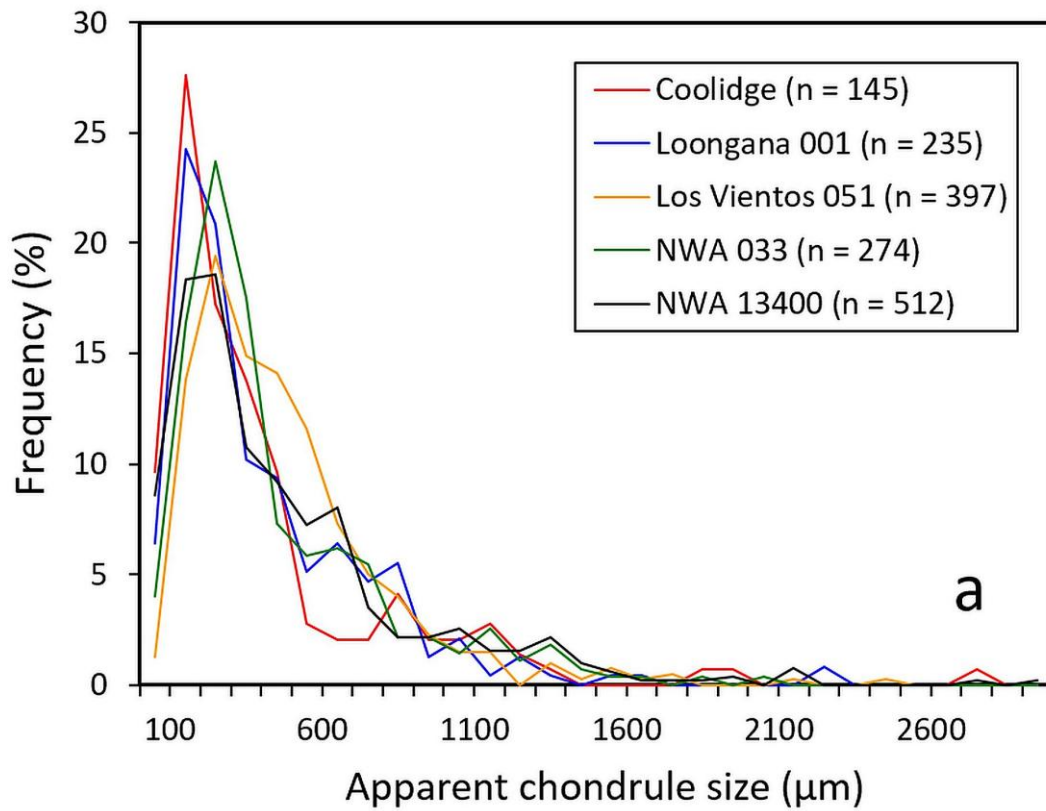


Fig. 5

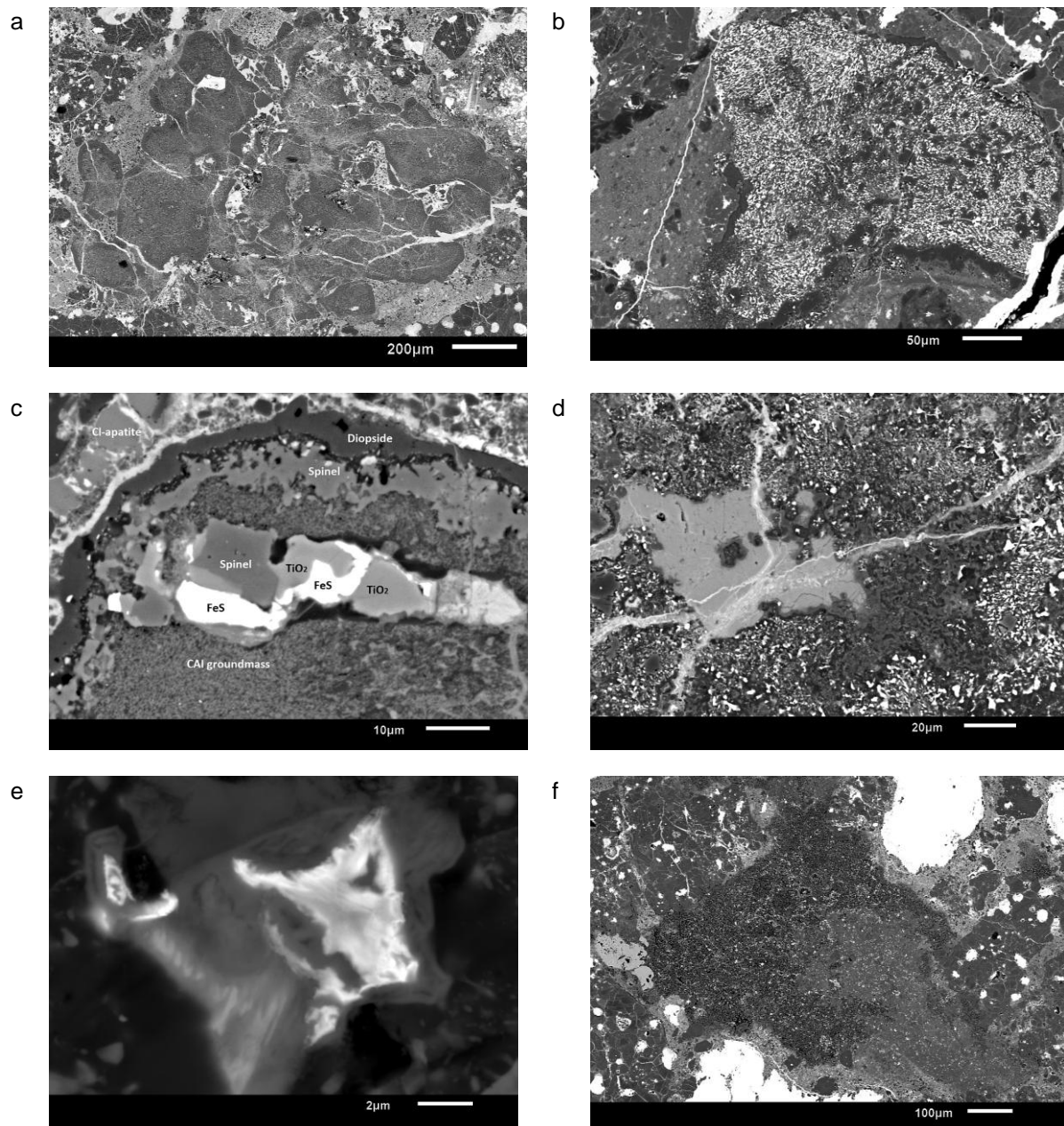


Fig. 6.

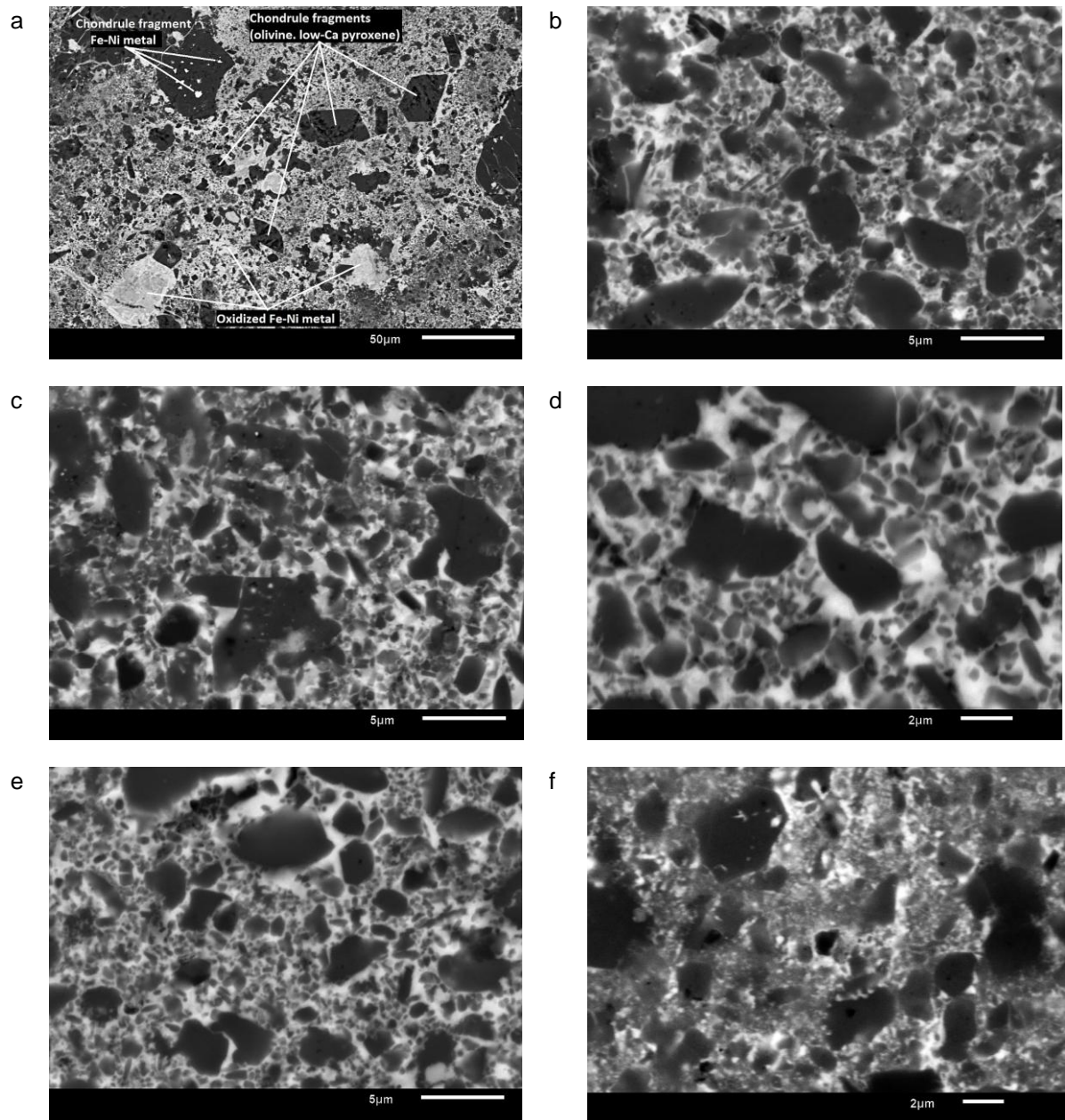


Fig. 7

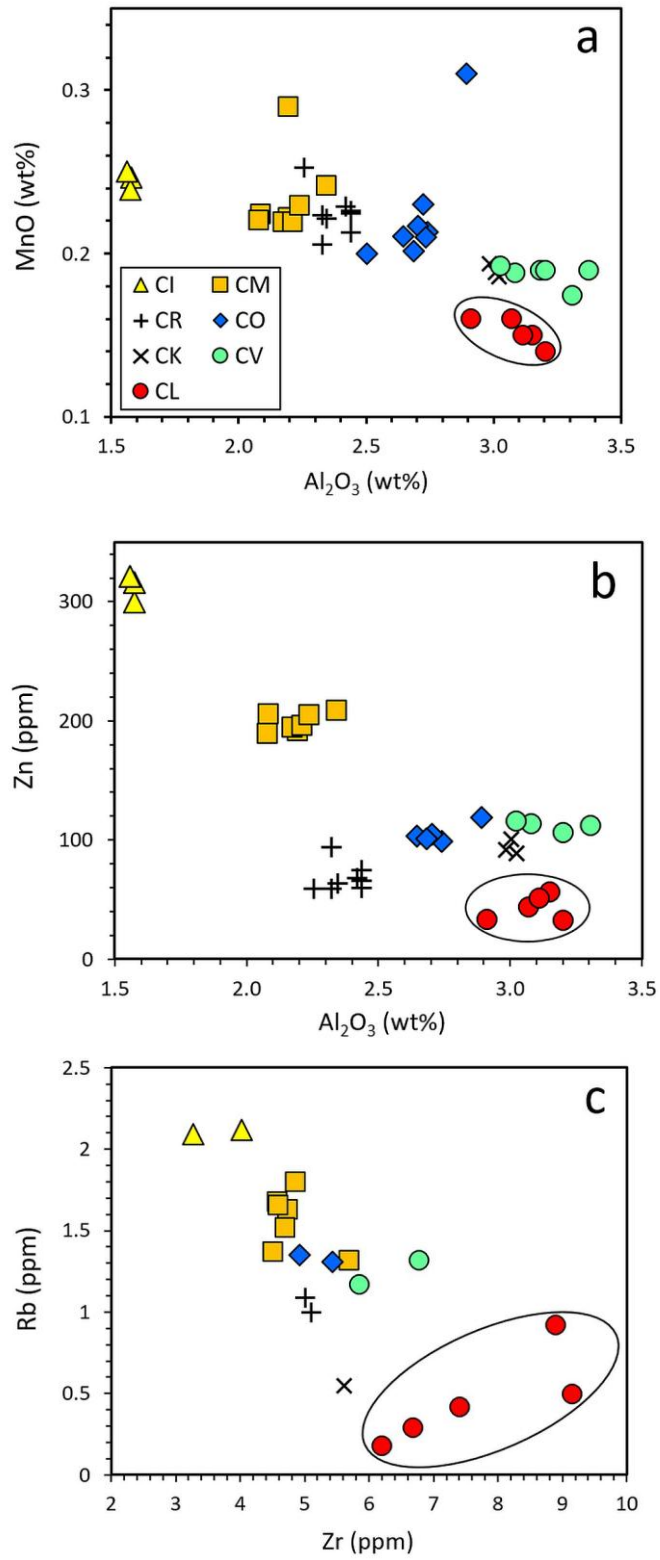


Fig. 8

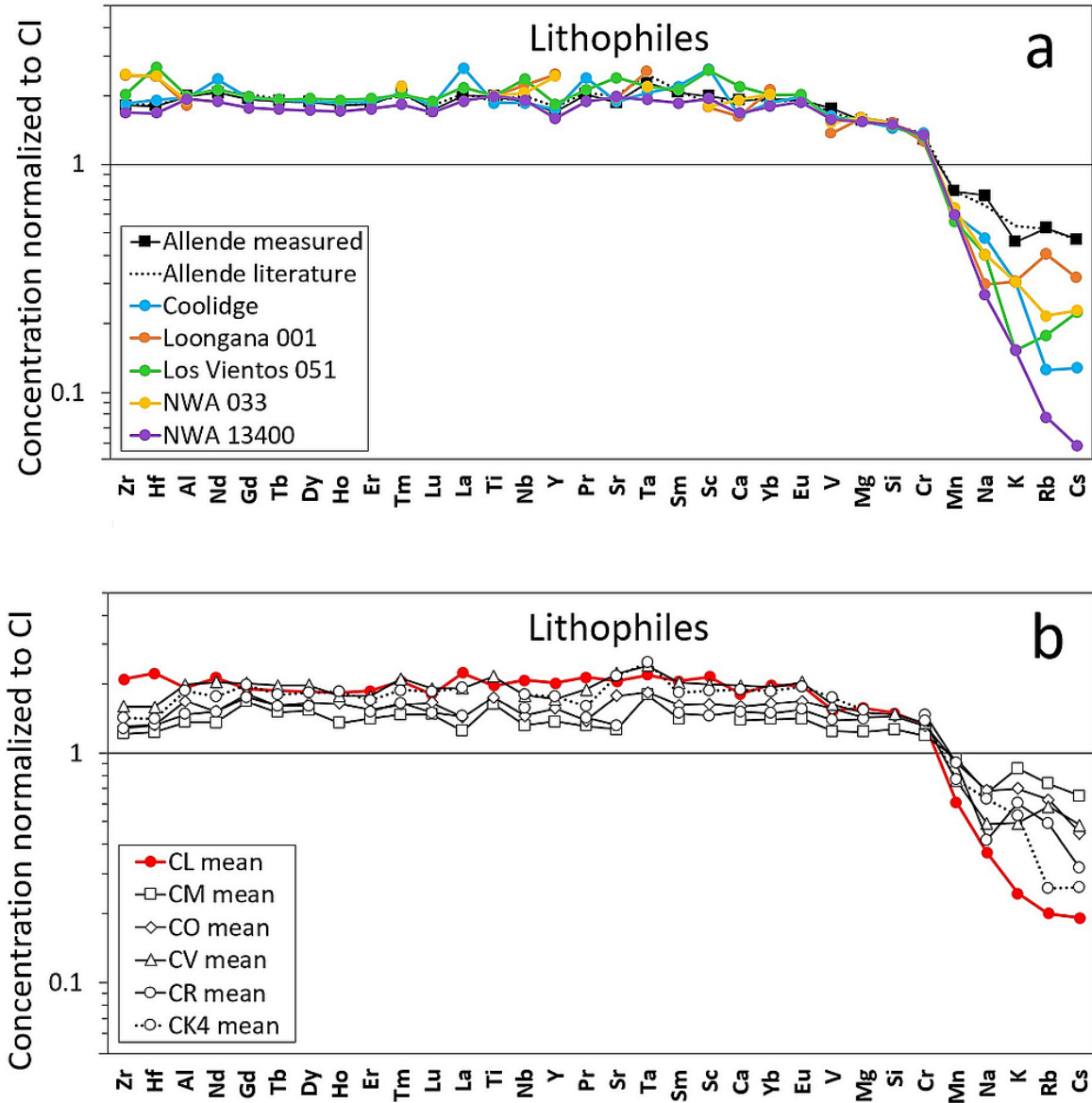


Fig. 9

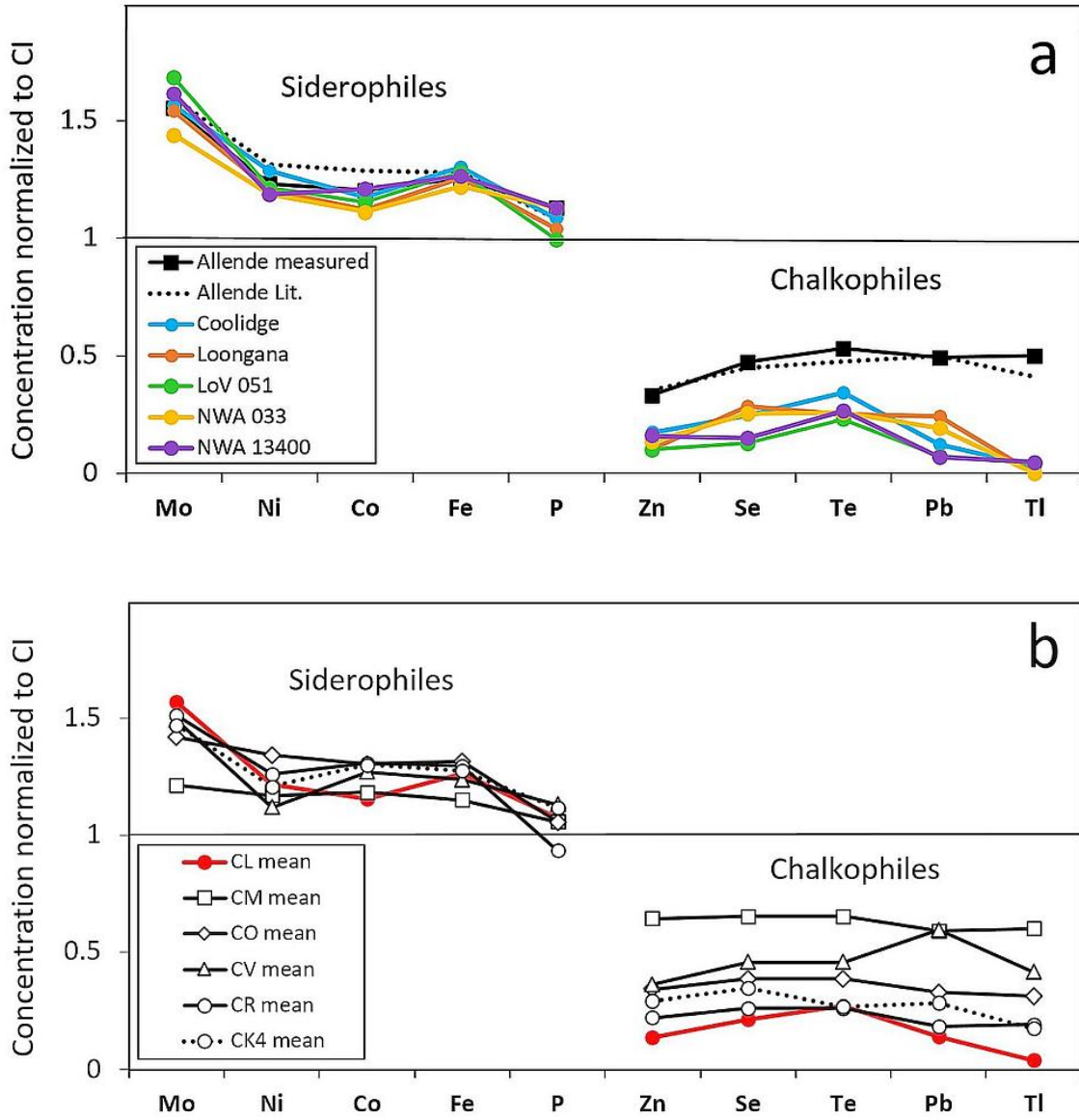


Fig. 10

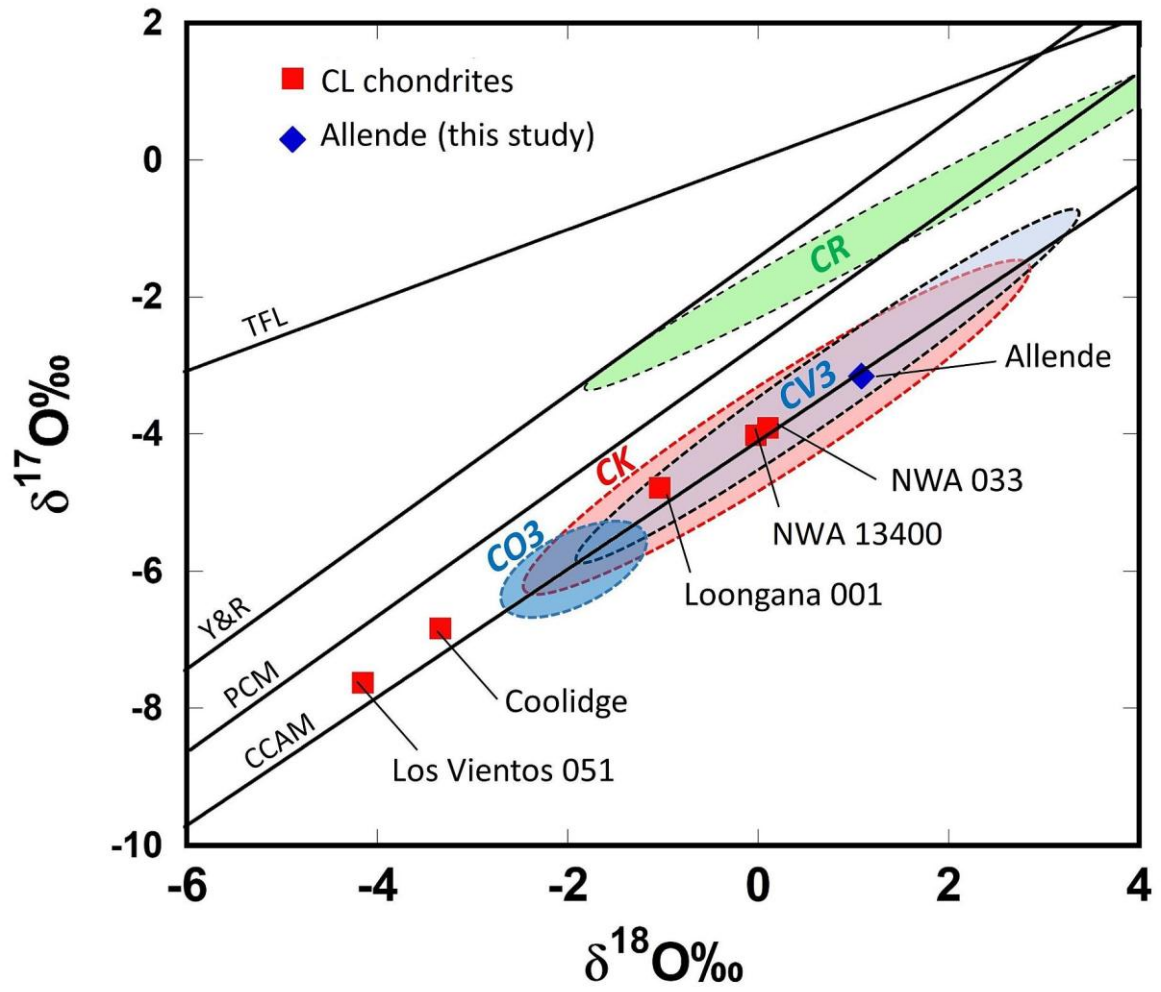


Fig. 11

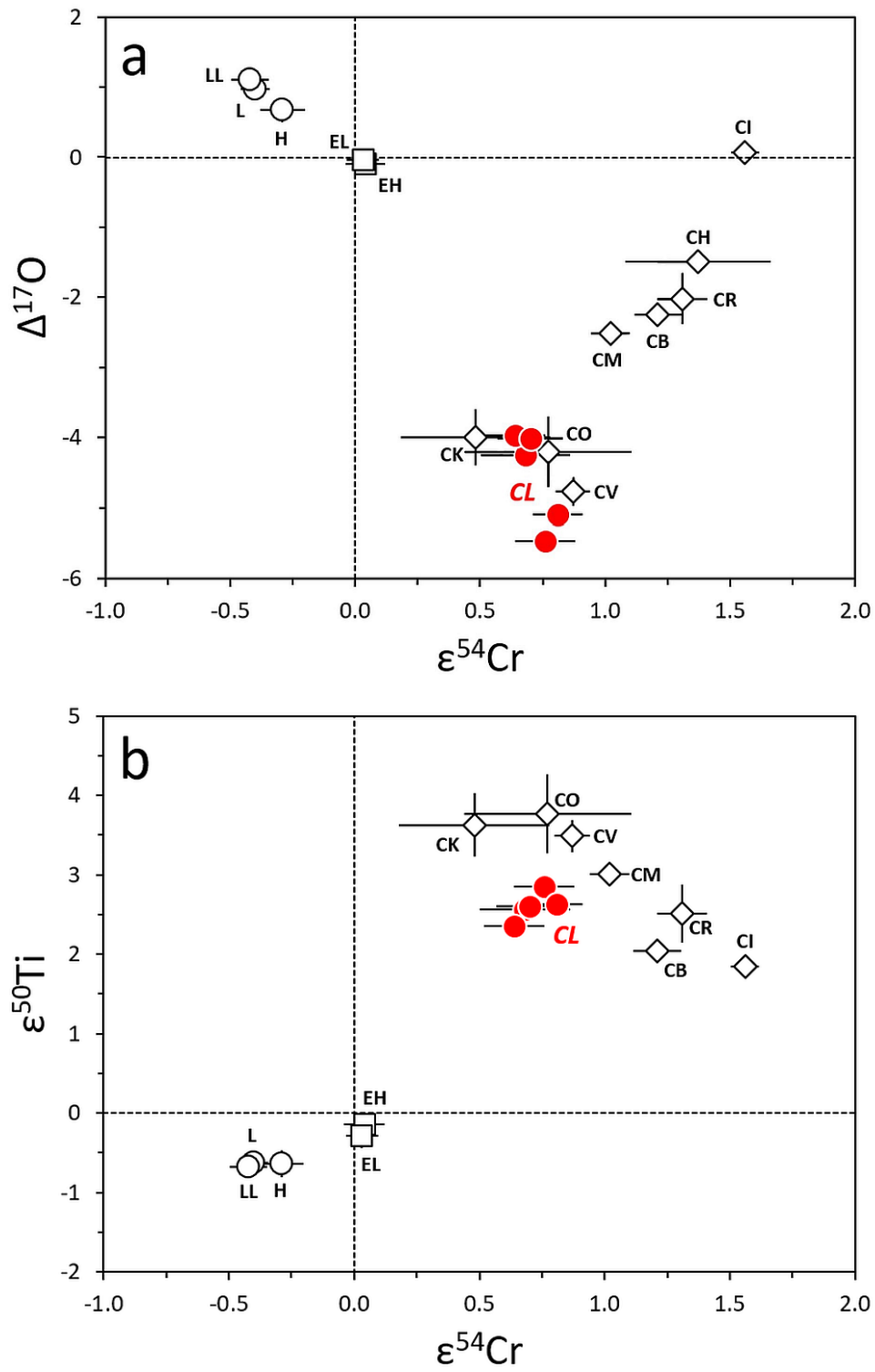


Fig. 12

Electronic Annex

[Click here to download Electronic Annex: Research_data_2D_chondrule_sizes.xlsx.xlsx](#)